

# Structural constraints limit the regime of optimal flux in autocatalytic reaction networks

Armand Despons,<sup>1</sup> Yannick De Decker,<sup>2</sup> and David Lacoste<sup>1</sup>

<sup>1</sup>*Gulliver Laboratory, UMR CNRS 7083, PSL Research University, ESPCI, Paris F-75231, France*

<sup>2</sup>*Center for Nonlinear Phenomena and Complex Systems (CENOLI),  
Université libre de Bruxelles (ULB), Campus Plaine, C.P. 231, B-1050 Brussels, Belgium*

(Dated: June 6, 2023)

Autocatalytic chemical networks play a predominant role in a large number of natural systems such as in metabolic pathways and in ecological networks. In this work, we present a theoretical framework that identifies the thermodynamic conditions under which autocatalytic networks run optimally in a non-equilibrium stationary state. Our theory shows that the overall reaction associated with the network is aligned with the thermodynamic force that drives the system out of equilibrium. We also demonstrate that the thermodynamic force required to operate at a maximal flux obeys universal constraints that are independent of the kinetics, but solely determined by the stoichiometry of the overall process and by the structural properties of the underlying chemical reaction network.

The dynamical properties of most systems found in nature can be traced back to a combination of chemical reactions that are maintained out of equilibrium. This is particularly the case in biology and in ecology, where these chemical reaction networks can reach high levels of complexity. Many such networks involve autocatalysis, which is the ability of chemicals to catalyze their own formation [1, 2]. Autocatalysis enables exponential growth [3, 4], self-replication [5], and metabolism [6].

The properties of chemical reaction networks are constrained by non-equilibrium thermodynamics. For example, living systems are thought to self-organize thanks to energy and matter flows, which allow them to lower their own entropy at the expense of an entropy increase in the environment [7], as required by the second law. Thermodynamics is also believed to play a key role in chemical evolution [8, 9] and in the organization of ecological communities [10, 11]. Yet, understanding precisely the role played by thermodynamic constraints proved difficult both for biology and ecology, despite the many recent efforts on this issue [12–16]. Because of this, we still do not fully understand the fundamental principles by which chemical evolution operates, which limits our ability to design new materials with life-like properties.

This lack of general understanding also has more practical consequences. The knowledge we have about metabolic networks is rather limited as far as kinetics is concerned. For this reason, current modelling approaches for metabolic networks focus on predicting steady fluxes by optimizing an objective function with linear constraints, as in Flux Balance Analysis (FBA) [17, 18] or in Structural Kinetic Modeling (SKM) [19]. These methods are general, valid for any chemical network and do not require a detailed knowledge of the kinetics, but it is not easy to use them to make predictions about metabolite concentrations or to assess from them the robustness of the network.

The aforementioned problems are all related to the fact

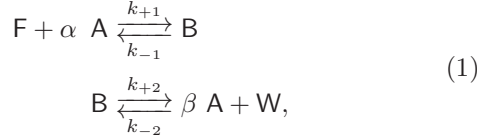
that while non-equilibrium thermodynamics is a well-established discipline, its implications for autocatalytic networks have not been fully explored yet. In this context, we prove here the existence of previously unknown constraints that thermodynamics puts on the dynamical properties of autocatalytic reaction networks.

Our result is obtained by developing a theoretical framework that is dedicated to the study of autocatalytic chemical networks in a stationary non-equilibrium regime. This approach builds on a recent stoichiometric classification of autocatalytic chemical networks [20, 21], which can be used to identify such networks thanks to chemoinformatic techniques [22–24]. We find that there is a fundamental connection between the topology of a network, the stoichiometry of its autocatalytic reactions, and the thermodynamic force keeping this network out of equilibrium. Based on this, we show that the force required to operate an autocatalytic network at a maximum rate obeys universal constraints, which depend on topology and stoichiometry, but are independent from the kinetics of all the reactions involved. Because these constraints contain information on the topology of the network, they can be used to rule out certain network architectures for a given global autocatalytic reaction, even in the absence of any knowledge about kinetics. Our framework also suggests a mechanism by which robustness and chemical selection could emerge in out-of-equilibrium chemical networks.

## MOTIVATING EXAMPLE

### A simple autocatalytic system

Consider, for illustration, the following reactive system:



with  $\beta > \alpha > 0$ . The topology of (1) is encoded in its stoichiometric matrix,

$$\nabla = \begin{array}{c} \text{F} \\ \text{W} \\ \text{A} \\ \text{B} \end{array} \begin{array}{cc} \begin{pmatrix} -1 & 0 \\ 0 & 1 \\ -\alpha & \beta \\ 1 & -1 \end{pmatrix} \\ \begin{matrix} 1 & 2 \end{matrix} \end{array}. \tag{2}$$

The species F and W act as fuel and waste for the overall production of the other species. In what follows, we will treat their concentrations,  $f$  and  $w$ , as constants.

Only a submatrix of (2) is required to capture the autocatalytic behavior of (1):

$$\mathbb{S} = \begin{array}{c} \text{A} \\ \text{B} \end{array} \begin{array}{cc} \begin{pmatrix} -\alpha & \beta \\ 1 & -1 \end{pmatrix} \\ \begin{matrix} 1 & 2 \end{matrix} \end{array}. \tag{3}$$

This submatrix establishes a connection between the time derivative of the concentrations of the *autocatalytic species*  $a$  and  $b$  with the reaction fluxes,

$$\text{d}_t \begin{pmatrix} a \\ b \end{pmatrix} = \mathbb{S} \cdot \mathbf{j}, \tag{4}$$

where  $\mathbf{j}$  is a vector containing the fluxes of reactions 1 and 2,  $\mathbf{j} = (j_1, j_2)^\top$ . For ideal isothermal systems, each of these reaction fluxes can be decomposed as the difference of two one-way fluxes obeying the law of mass action:

$$j_{+1} = k_{+1} f a^\alpha, \quad j_{-1} = k_{-1} b, \tag{5}$$

$$j_{+2} = k_{+2} b, \quad j_{-2} = k_{-2} a^\beta w. \tag{6}$$

Nothing prevents this reactive system from reaching the equilibrium state, since the concentrations of both A and B are unconstrained. To drive the network (1) away from its equilibrium state, we introduce a control mechanism (*i.e.* a chemostat) which maintains the concentrations  $a$  or  $b$  constant thanks to an outgoing flux  $\mathcal{J}$  as shown in Figure 1.

### Control of species A

When the concentration of species A is controlled in that way, the steady state is such that  $j_1 = j_2$ , which shows that there is a *tight coupling* [25] between the two reactions. Here,  $j_1$  and  $j_2$  are also equal to the production rate  $\mathcal{J}$  of the overall reaction:



This reaction has an overall affinity (which is equal to the opposite of the Gibbs free energy  $\Delta G$ )  $\mathcal{A} = \mu_F - \mu_W - (\beta - \alpha) \mu_A$ , where  $\mu_i$  is the chemical potential of species  $i$ . Since  $\mu_F$  and  $\mu_W$  are fixed, fixing  $\mu_A$  is essential to maintain the system in a non-equilibrium state where  $\mathcal{A}$  is non-zero. Otherwise, the system will reach equilibrium, where the affinity vanishes.

The steady global production rate:

$$\mathcal{J} = \frac{k_{+1} k_{+2}}{k_{-1} + k_{+2}} \left[ a^\alpha f - \left( \frac{k_{-1} k_{-2}}{k_{+1} k_{+2}} \right) a^\beta w \right]. \tag{8}$$

Introducing the reaction quotient  $Q = a^{(\beta-\alpha)} w/f$  and the equilibrium constant  $K = k_{+1} k_{+2}/k_{-1} k_{-2}$  of the global reaction (7), it is easy to show that the global flux  $\mathcal{J}$  has the same sign as the affinity, since  $\mathcal{A} = \ln(K/Q)$  (we work with units where  $RT = 1$ ). In other words, the global flux is aligned with the thermodynamic force.

At low values of  $Q$ , forward reactions make this flux an increasing function of  $Q$  while at high values of  $Q$ , it is a decreasing function due to backward reactions. In between, the global flux goes through a maximum at a value  $Q = Q^* = K \times \alpha/\beta$ . Thus, the maximum flux is reached when the chemical affinity becomes

$$\mathcal{A}^* = \ln \frac{\beta}{\alpha}. \tag{9}$$

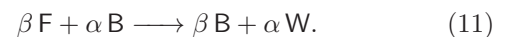
Hence, the distance from equilibrium at which the autocatalytic network achieves its optimal production rate, namely  $\mathcal{A}^*$ , is not fixed by the values of kinetic constants or by the equilibrium constant of the global process. It only depends on the stoichiometry of the overall reaction. We illustrate these results in Fig. 1, for the case  $\alpha = 1, \beta = 2$ . Note that this condition on the affinity can also be expressed in terms of the concentration  $a$ . Since  $\exp(\mathcal{A}^*) = K/Q^*$ , the point of maximum flux is given by

$$\left( \frac{a^*}{a_{\text{eq}}} \right)^{\beta-\alpha} = \frac{\alpha}{\beta}. \tag{10}$$

For the example considered in Fig. 1, this means that optimality is reached when the concentration of the chemostat is at half its equilibrium value.

### Control of species B

We can carry a similar analysis if, instead of A, B is the controlled autocatalytic species. One finds that the steady state is such that  $j_1/\beta = j_2/\alpha = \mathcal{J}$ , which is the overall production rate of species B,



The steady-state solution now involves polynomials of different order, making it impossible to find explicitly

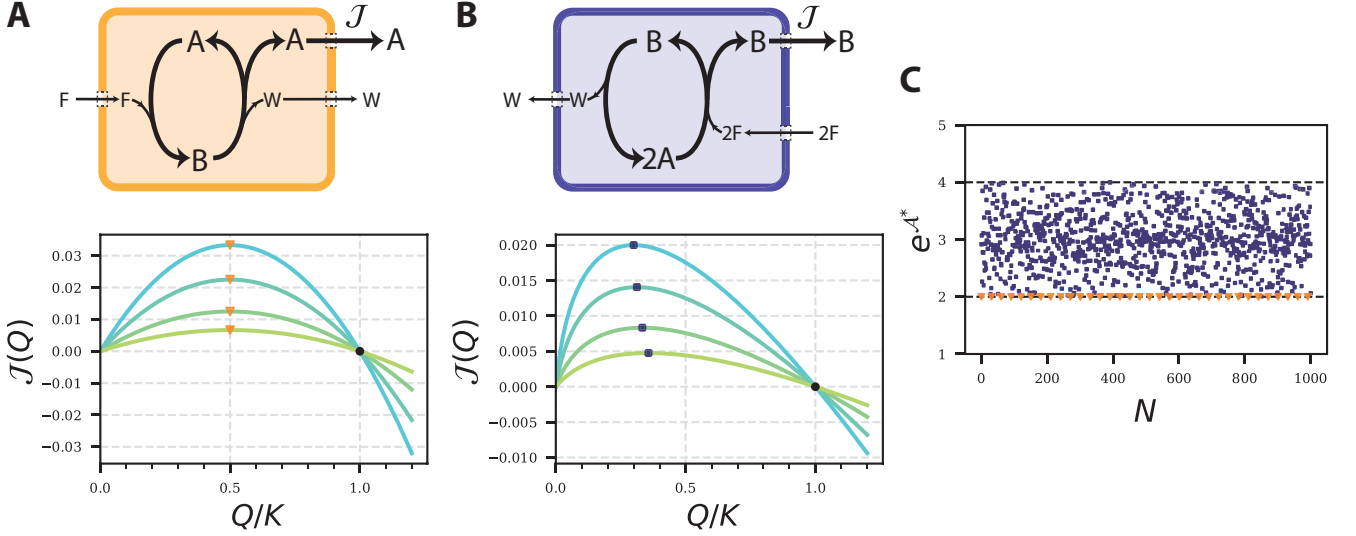


**Figure 1:** This figure shows selected properties of the autocatalytic system (1) for  $\alpha = 1$  and  $\beta = 2$ . **(A)** The top figure represents a reactor in which the concentrations of F, W and A are maintained constant thanks to exchanges with external reservoirs (chemostats). In the bottom figure, the global flux  $\mathcal{J}$  vanishes when  $Q = K$  (on the black circle) and reaches a maximum at the same location  $Q^* = K/2$  (on black triangles), irrespectively of the choice of rate constants. **(B)** Now, F, W are still chemostatted, but now B is chemostatted instead of A, as shown in the top figure. Now the maxima of the global reaction rate are reached at different locations such that  $Q^* \leq K/2$ . Note that all the fluxes still vanish at  $Q = K$ . **(C)** Bound for the exponential of the global affinity  $\mathcal{A}^*$ , for randomly chosen sets of kinetic rate constants indexed by  $N$ . When species A is controlled (orange triangles), the optimal affinity is always given by  $\ln 2$ , as explained in the text. When species B controlled (blue squares),  $\ln 2$  becomes a lower bound. In addition, in that case, the affinity is also upper-bounded by  $\ln 4$ , a property specific to this particular case, which is explained in the Supplementary Materials.

the conditions maximizing the rate of production with the previous method. Nonetheless, we can determine  $\mathcal{A}^*$  by numerically finding the value of  $Q^*$  that maximizes the global reaction rate for randomly generated values of the various kinetic constants. We find that the optimal affinity is now bounded from below:

$$\mathcal{A}^* \geq \ln \frac{\beta}{\alpha}, \quad (12)$$

as shown in Figure 1.B-C for  $\alpha = 1$  and  $\beta = 2$ . For these particular values of  $\alpha$  and  $\beta$ , the inequality (12) can also be derived analytically (see [SI Appendix Section 1](#)). Here too, the constraint acting on the optimal distance from equilibrium solely depends on the stoichiometry of the overall reaction.

This thermodynamic constraint translates into a threshold for the value of the concentration of the controlled species,  $b^*$  as

$$\left( \frac{b^*}{b_{\text{eq}}} \right)^{\beta-\alpha} \leq \frac{\alpha}{\beta}, \quad (13)$$

where  $b_{\text{eq}}$  is the equilibrium concentration of B. Note the importance of the condition  $\beta > \alpha > 0$ , which guarantees the invertibility of the stoichiometric matrix  $\mathbb{S}$  and leads to useful equalities or inequalities Eqs. (10)-(13).

## GENERAL APPROACH FOR AUTOCATALYTIC CHEMICAL REACTION NETWORKS (CRNS)

In what follows, we present a general approach that enables the computation of the overall affinity  $\mathcal{A}^*$  corresponding to a condition of local extremum of the global production rate. Our method relies on the stoichiometry of the reaction network, and circumvents the need to explicitly evaluate the steady states or reaction rates of the system under consideration.

### Stoichiometric analysis of autocatalytic CRNs

Following a recent stoichiometric characterization of autocatalysis [20], a general autocatalytic network should contain one or several *autocatalytic cores*. An essential feature of these cores is that they are described by an invertible stoichiometric sub-matrix, which makes the corresponding subnetwork a deficiency zero network [26]. The existence of this invertible sub-matrix is a sufficient condition for autocatalysis, which implies the absence of conservation laws [13, 27, 28] thanks to Gordan's theorem [20]. In the following, we assume that the full stoichiometric matrix  $\nabla$  contains a square submatrix  $\mathbb{S}$  that is

invertible (see (69) in the Materials and Methods section). Reactions of  $\mathbb{S}$  will be called *autocatalytic reactions*, species of  $\mathbb{S}$  will be called autocatalytic species, while other species will be called *external*.

Similar to the example above, the concentrations of all external species are assumed to be constant, either because these species are in excess, which is typically the case for food or fuel species or because these species are catalysts. Given the structure of the full stoichiometric matrix of (69), one can show that the network can still be in detailed balance (see (36) and [SI Appendix Section 2.1](#)). To break detailed balance, in addition, the concentration of at least one of the autocatalytic species should be controlled, by actively maintaining its concentration constant with an outgoing flux.

We call this special species  $X$ , and the remaining non-controlled autocatalytic species are denoted by  $Y$ . The stoichiometric matrix  $\mathbb{S}$  splits into a row vector  $\mathbf{S}^X$  and a matrix  $\mathbb{S}^Y$  [27]:

$$\mathbb{S} = \begin{pmatrix} \mathbf{S}^X \\ \mathbb{S}^Y \end{pmatrix}. \quad (14)$$

The corresponding kinetic equations are given by

$$d_t x = \mathbf{S}^X \cdot \mathbf{j} + I = 0 \quad (15)$$

$$d_t \mathbf{y} = \mathbb{S}^Y \cdot \mathbf{j}, \quad (16)$$

where  $x$  denotes the concentration of the  $X$  species and  $\mathbf{y}$  is the concentration vector of all the  $Y$  species. The vector  $\mathbf{j}$  contains the rates of the autocatalytic reactions, and  $I$  is a scalar function describing the exchange of matter with the chemostat.

The inverse  $\mathbb{S}^{-1}$  plays an important role:

$$\mathbb{S}^{-1} = \{\mathbf{g}_\sigma\}_{Z_\sigma \in \mathcal{Z}}, \quad (17)$$

where  $\mathbf{g}_\sigma$  is the column of  $\mathbb{S}^{-1}$  associated to species  $Z_\sigma$ , which denotes autocatalytic species of the  $X$  or of the  $Y$  type, and  $\mathcal{Z}$  is the set of all the autocatalytic species. It follows from the property of the inverse that  $\mathbf{g}_\sigma$  represents a reaction pathway that produces a single unit of species  $Z_\sigma$  without affecting the other species (see [SI Appendix Section 2.2](#)). For this reason,  $\mathbf{g}_\sigma$  is the *elementary mode of production* of species  $Z_\sigma$  [20]. From all the elementary modes of production, one can build a reaction vector  $\mathbf{g} \equiv \sum_\sigma \mathbf{g}_\sigma$ , which represents a combination of elementary modes that increases the amount of all the autocatalytic species by one unit:

$$\mathbb{S} \cdot \mathbf{g} = \mathbf{1}, \quad (18)$$

where  $\mathbf{1}$  is a column vector full of ones. The existence of this vector is a sufficient condition for autocatalysis.

The steady-state of (16) is a vector belonging to the left nullspace of  $\mathbb{S}^Y$  [27, 28], which is spanned by  $\mathbf{g}_X$ ,

the elementary mode of production associated to the  $X$ -species. Thus, the stationary flux vector can be written as

$$\mathbf{j} = \mathcal{J} \mathbf{g}_X, \quad (19)$$

which expresses a *tight coupling* condition, since all stationary fluxes are proportional to the same function  $\mathcal{J}$ .

### Kinetics and thermodynamics of the CRN

We now introduce assumptions about the dynamics of the network at the level of elementary reactions. Every such reaction denoted  $\rho$  is assumed to be reversible, with a net flux given by

$$j_\rho = j_{+\rho} - j_{-\rho}. \quad (20)$$

Here, one-way fluxes  $j_{\pm\rho}$  obey mass-action kinetics [26, 29]:

$$j_{\pm\rho} = k_{\pm\rho} \prod_\sigma z_\sigma^{S_{\pm\rho}^\sigma}, \quad (21)$$

where  $z_\sigma$  is the concentration of species  $Z_\sigma$ , and  $\mathbb{S}_+$  (resp.  $\mathbb{S}_-$ ) is the stoichiometric matrix associated to forward (resp. reverse) reactions, such that  $\mathbb{S} = \mathbb{S}_- - \mathbb{S}_+$ . Note that the constant concentrations of the fuel/food species have been absorbed in the effective rate constants  $k_{\pm\rho}$ . We choose to work with ideal systems for clarity of presentation, but we show in the Supplemental Materials ([SI Appendix Section 3.2](#)) that the results presented below remain valid for non-ideal solutions.

Then, as in the examples, one can show that the affinity of the network at a macroscopic scale can be written as the logarithm of the ratio of an effective equilibrium constant  $K$  and a reaction quotient  $Q$  [30]:

$$\mathcal{A} = \ln \left( \frac{K}{Q} \right). \quad (22)$$

Here, the reaction quotient is simply given by the concentration of the controlled autocatalytic species ( $Q = x$ ) and the stationary global flux is a function of this quantity,  $\mathcal{J} = \mathcal{J}(Q)$ .

We expect that in the cases of interest, this flux will present at least one maximum when the CRN is brought out of equilibrium. Indeed, due to the tight coupling condition, the total entropy production rate (EPR) has a simple expression [13, 27, 28]:

$$\Sigma = \mathcal{J} \mathcal{A}. \quad (23)$$

The second law of thermodynamics dictates that  $\Sigma \geq 0$ , and equality is achieved at equilibrium, where both  $\mathcal{J}$  and  $\mathcal{A}$  vanish. It follows, from (22), that  $\mathcal{J}(Q) \geq 0$  when  $Q \in [0, K]$ . Let us consider a class of autocatalytic

networks, for which the  $X$  species has a nucleating role [23]. In that case, the flux  $\mathcal{J}(0)$  is zero when this species is absent (in other words, for  $Q = 0$ ). This was the case, for example, with the simple autocatalytic system discussed earlier (see Figure 1). For these networks, there must be at least one local extremum of the global flux in the interval  $Q \in [0, K]$ . This regime is optimal, in the sense that the  $X$  species is produced at a maximal rate. Importantly, the extremum of the global flux and that of the EPR do not coincide because  $\mathcal{A}$  in (22) is a non-linear function of  $Q$  which also enters in (23). This is in agreement with the observation that the optimal regime of operation of non-equilibrium systems generally do not correspond to a point where the EPR is extremum [31].

We now focus on an extremal point where the derivative of the global flux vanishes:  $d_Q \mathcal{J} = 0$ . Due to the tight coupling condition, (19), all reaction fluxes are also at an extremum, thus  $d_Q j_\rho = d_Q j_{+\rho} - d_Q j_{-\rho} = 0$  as well. To characterize this configuration, we introduce the log-derivative of the stationary elementary fluxes, which we call  $F_{\pm\rho}$ :

$$F_{\pm\rho} = d_Q \ln j_{\pm\rho} = \sum_{\sigma} S_{\pm\rho}^{\sigma} d_Q \ln z_{\sigma}. \quad (24)$$

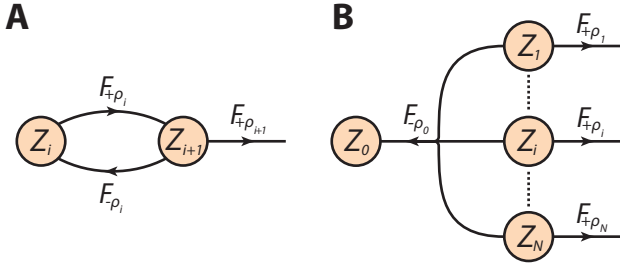


**Figure 2:** Representation of the structural constraints (25). **(A)** For any reaction  $\rho_i$  consuming species  $Z_i$ , we can write the two unidirectional transitions as  $\pm\rho_i$ . If one considers a *linear pathway* where a single species  $Z_i$  produces, via  $+\rho_i$ , one species  $Z_{i+1}$ , then  $\ln j_{-\rho_i}$  and  $\ln j_{+\rho_{i+1}}$  are both equal (up to a constant additive term). **(B)** For a *branched pathway* a species  $Z_0$  splits, via  $+\rho_0$ , to create various species indexed by  $i$ ,  $Z_i$ . The logarithm of the reverse flux  $\ln j_{-\rho_0}$  becomes (up to a constant additive term), the sum of the log-concentration of species  $Z_i$  ( $\ln z_i$ ) weighted by their multiplicity given by  $S_{-\rho_0}^i$ .

The  $F_{\pm\rho}$ s quantify the response of the steady unidirectional flux ( $j_{\pm\rho}$ ) with respect to a change in non-equilibrium constraints. Because the  $F_{\pm\rho}$  are log-derivatives, all the factors entering rate laws that do not depend on  $Q$  will not contribute to these coefficients. This includes the rate constants, which do not appear explicitly. Remarkably, the coefficients  $F_{\pm\rho}$ s satisfy structural constraints related to the topology of the network. A graphical illustration of these structural relations is provided in Fig. 2 for the particular case of a linear and a branched reaction pathway. For a general network, these

structural relations take a form analogous to Kirchoff's laws:

$$\mathbf{F}_- = \mathbf{F}_+ \cdot (\mathbb{S}_+^{-1} \cdot \mathbb{S}_-), \quad (25)$$

provided  $\mathbb{S}_+$  is invertible, which is the case in most networks of interest.

These coefficients  $F_{\pm\rho}$ s play a key role in our theory because the value  $\mathcal{A}^*$  of the affinity at the optimal point  $Q = Q^*$  can be expressed only in terms of the  $F_{\pm\rho}^*$  at that point according to:

$$\mathcal{A}^* = \sum_{\rho} g_{\rho}^{\rho} \ln \left( \frac{F_{-\rho}^*}{F_{+\rho}^*} \right). \quad (26)$$

Thus, the bounds on  $\mathcal{A}^*$  and the optimal values taken by the response coefficients  $F_{\pm\rho}^*$ s can be obtained by solving a convex optimization problem with (25) as linear constraints and (44) as additional non-linear constraints coming directly from the tight coupling condition. The solution to this optimization problem connects thermodynamic quantities in an optimal regime of autocatalytic growth with the topology of the reaction network. Importantly, this link does not rely on an explicit evaluation of the steady-state fluxes or of concentrations, nor does it require a knowledge of kinetic parameters. This is our first main result.

#### Bounds on the cycle affinity in the maximum flux configuration

Since the bounds on the optimal affinity do not depend explicitly on the expressions for the steady-state concentrations or reaction rates, our method is applicable to large and complex networks, in which these concentrations and rates are too complex to be computed. For the same reason, the bounds hold even if the system features multistability, which is often found in autocatalytic networks [1]. We show this explicitly for the bistable Schlögl model [32] in the Supplementary Material (*SI Appendix Section 5.3*).

As an illustration of our approach, we derive lower bounds satisfied by the global affinity of the Hinshelwood autocatalytic cycle [33] (see Fig. 3.A and Supplementary materials (*SI Appendix Section 5.2*)). When species B or D is controlled, one finds:

$$\mathcal{A}^* \geq \ln 4, \quad (27)$$

which is a tight bound that can be approached as closely as desired with an appropriate choice of rate constants, as shown in Figure 3.D. When, instead, the concentration of A or C is maintained constant, one finds that there is no extremum for the global flux,  $\mathcal{J}$  is a decreasing function of  $Q$  whose largest value occurs at  $Q = 0$  (see Figure 3). As a result,  $\exp(\mathcal{A}^*)$  diverges.



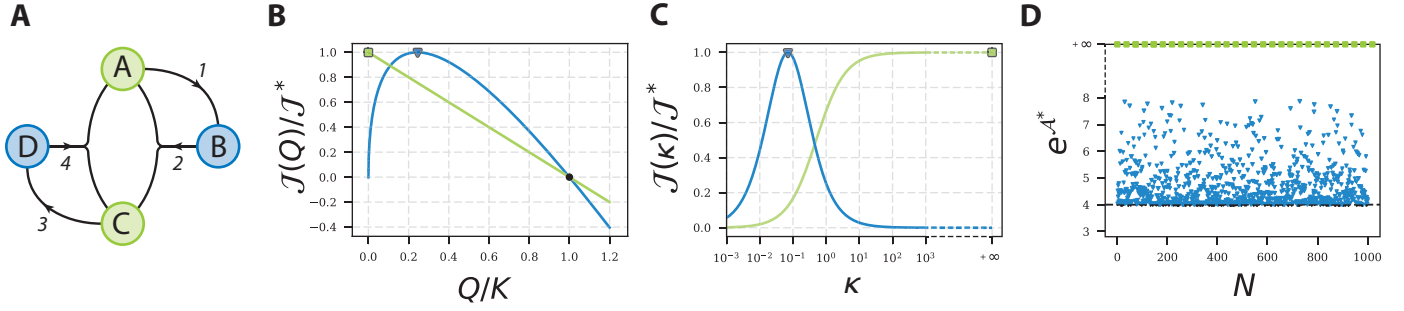


**Figure 3:** Optimal properties of the Hinshelwood cycle. **(A)** Schematic representation of the Hinshelwood cycle with two types of species: green species (A or C) and blue species (B or D). **(B)** Global flux normalized by its maximum value  $\mathcal{J}^*$  as a function of  $Q/K$  when a specific species of the cycle is chemostatted. This flux vanishes at equilibrium (black dot) and has an extremum (blue triangle) if a blue species is chemostatted or simply reaches its maximal value at  $Q = 0$  (green square) if a green species is chemostatted. **(C)** Global flux normalized by its maximum value  $\mathcal{J}^*$  as a function of the degradation rate  $\kappa$  of a specific species. When a blue species is targeted by degradation, an extremum exists and is reached at a finite value of  $\kappa$ . While, if a green species is targeted, the global flux is monotonously increasing and reaches its maximal value at infinity. **(D)** Despite differences in the setups with chemostats and with degradation, the global affinity at the optimum follows the same trend: for blue species,  $\mathcal{A}^*$  is lower-bounded by  $\ln 4$  (blue Triangles) whereas for green species, it diverges (green squares) when rate constants are chosen randomly and indexed by  $N$ . Simulation parameters for Figs. **(B)** and **(C)** are  $k_{+1} = k_{+3} = 1$  and  $k_{+2} = k_{+4} = k_{-1} = k_{-2} = k_{-3} = k_{-4} = 0.1$ .

More examples are considered in Supplementary materials (*SI Appendix Section 4.1 & 4.2*), notably we analyze arbitrary  $3 \times 3$  networks, covering all the autocatalytic motifs described in [20]. In what follows, we focus on general conclusions that can be drawn for some classes of autocatalytic networks.

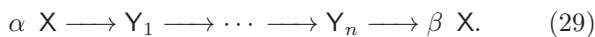
### General principles concerning the production of the autocatalytic species

Here, we show that two situations emerge, depending on whether or not the  $X$  species appears as a reactant.

*Seed-dependent mode of production* We call *seed-dependent* [22, 23] a mode of production for which species  $X$  is needed to start the reaction. This corresponds to an overall equation given by



with  $\alpha$  and  $\beta$  being integers such that  $\beta > \alpha > 0$ , and the  $(\diamond)$  symbol represents all the spectator species. Remember also that in our formalism, the concentrations of the fuel/food species  $F$  and  $W$  are absorbed in the rate constants, so that these species do not appear explicitly in the stoichiometric equations. The simplest network leading to (28) is a generalized version of the Type I core as shown in Supplementary materials (*SI Appendix Section 4.4*):



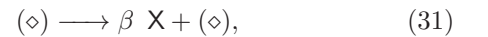
In that case,  $\mathcal{J}$  has a maximum for:

$$\mathcal{A}^* = \ln \left( \frac{\beta}{\alpha} \right). \quad (30)$$

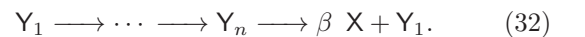
It turns out that, for networks without *back-branches* (see *SI Appendix Section 4.2* and the supplemental information of [20] for a definition) and admitting (28) as overall equation, (30) is the lowest achievable bound. We surmise this is not restricted to this specific class of networks and holds in general for arbitrary autocatalytic networks. As a consequence, we conjecture that:

*Along a seed-dependent mode of production whose overall equation is  $\alpha X + (\diamond) \longrightarrow \beta X + (\diamond)$ , the global affinity associated to the optimal flux is lower-bounded by  $\ln(\beta/\alpha)$ .*

*Seed-independent mode of production.* Conversely, we call *seed-independent* a mode of production, for which species  $X$  is not needed to start the reaction. This corresponds to



where  $\beta$  is a positive integer. The *simplest* topology compatible with (31) is



The latter is a generalization of the Type II network studied in Supplementary materials (*SI Appendix Section 4.5*). Its optimal affinity  $\mathcal{A}^*$  reads:

$$\mathcal{A}^* = \ln(\beta + 1). \quad (33)$$

The overall reaction associated with seed-independent production (31) is quite general and could potentially describe a large panel of reaction networks, including non-autocatalytic ones. However, we emphasize that the

existence of an optimal flux and the bounds on the corresponding affinity can only exist if an underlying autocatalytic network is present. Again, (33) is the lowest achievable bound for networks without *back-branches* and having (31) as overall equation. Hence, as before, we conjecture that:

*Along a seed-dependent mode of production whose overall equation is  $(\diamond) \longrightarrow \beta X + (\diamond)$ , the affinity where the global reaction flux is maximized is lower-bounded by  $\ln(\beta + 1)$ .*

We verified these two principles for the five simplest autocatalytic motifs derived in [20], the results are summarized in Table I in the Materials and Methods section below. The green (resp. blue) entries are those associated to a *seed-dependent* (resp. *seed-independent*) mode of production. Notably, the bounds derived in Table I remain valid if linear segments of reactions are added because such segments are not affecting the value of the bound (*SI Appendix Section 4.6*).

## DISCUSSION

We presented a theoretical framework that puts constraints on the affinity at which the rate of autocatalytic production is extremal. Remarkably, these constraints only depend on the topology of the underlying reaction network and are independent of the values taken by kinetic parameters. In this concluding section, we discuss how these results could be tested experimentally, we address their interpretation in terms of non-equilibrium thermodynamics and we present potential extensions of this work.

In practice controlling the concentration of a metabolite with an outgoing flux (i.e. chemostatting that species) can prove difficult, but a more manageable method of control might be to rely on selective degradation, which can be carried out by manipulating the system with light or temperature, or by using specific enzymes for instance. Enzymatic degradation is often described using Michaelis-Menten kinetics, which our model can account for as explained in the Materials and Methods section.

The property of tight coupling for the reaction fluxes is preserved in the presence of specific degradation of a species  $X$  (see (51)). One major difference with what happens with the concentration control is that now  $\mathcal{J}$  becomes function of the degradation rate constant  $\kappa$ , instead of  $Q$ . The global flux is zero for  $\kappa = 0$ , which corresponds to equilibrium, and also for a given  $\kappa_c$  (provided  $\kappa_c < \infty$ ), above which degradation overcomes the production of  $X$  by autocatalysis (see (55) in the Materials and Methods section). This threshold  $\kappa_c$  is experimentally accessible and has been considered before as a possible measure of fitness for autocatalytic networks [8].

The situation is thus similar to what happens with concentration control by chemostatting. We illustrated this point in Figure 3, for the Hinshelwood cycle. Figure 3.C shows that a maximal flux is reached for a finite value of  $\kappa$  when species B or C are being degraded. Furthermore, this maximum is only reached at infinity when A or D undergo degradation. The overall affinity associated to the reversible reactions of the autocatalytic network has the same bound as the one obtained with chemostatting (see Fig. 3.D and Materials and Methods section below).

Besides its interest for the design of autocatalytic or self-replicating systems [34], our approach suggests a method to obtain structural information from existing chemical networks. The idea would be to tune a flux associated to a given autocatalytic species as a function of a control parameter, which could be for instance the concentration or the degradation rate of that species. One would then adjust that parameter to the value that maximizes this flux. At this optimum point, one should measure either the global affinity or the concentration of the species which is being varied, the latter being typically more accessible in practice. By repeating this measurement for different realizations of the same network, one will obtain a cloud of points similar to that of Fig. 1 - possibly deformed due to additional constraints on rate constants. The bounds on this observed cloud of points then provides structural information which can be used to rule out certain autocatalytic networks.

The various bounds that we have encountered in this work measure how far from equilibrium a given network should be in order to deliver a maximal rate of autocatalytic production. It is advantageous for a given network to operate close to this point not only because the global reaction is fast, but also because the system is then robust: at this point, variations in the concentration of the autocatalytic species are buffered and hardly affect the flux, which is thus stable.

The affinity can also be interpreted as the entropy production associated with a steady production of  $X$  species [28] or, equivalently, as the production of entropy per autocatalytic cycle [8]. The bounds for the optimal affinities can thus be seen as the minimal cost required to maintain an optimal rate of autocatalytic production. We also observed that this minimal cost increases dramatically when certain reactions within the network are at equilibrium or when certain key species are depleted, as we have illustrated in the case of the Hinshelwood cycle. This is consistent with the idea that the thermodynamic cost should increase in a pathway when certain steps are at equilibrium [34, 35].

A natural extension of the present work would be to further investigate the thermodynamics of autocatalytic networks. It would be also interesting to explore possible connections between this work and a number of studies on thermodynamic trade-offs between dissipation, speed, and accuracy, and other recent studies on the response of

non-equilibrium Markovian systems to perturbations [36] and on universal thermodynamic bounds for symmetry breaking [37].

We observed that the bounds tend to increase with the topological complexity of the network as shown in Table I. One aspect of this topological complexity is the connectivity and in this respect, we have shown in Supplementary Materials that the bound indeed increases with the degree of branching of a reaction when the network contains only one such reaction (*SI Appendix Section 4.3*).

Finally, we note that autocatalytic systems are of particular importance for scenarios on the origin of life. Autocatalytic networks can amplify initially small numbers of molecules and the rate at which such species are produced would certainly play a role in the competition between molecules. In this context, running at an optimal and robust production rate could provide an autocatalytic network with a significant advantage in terms of chemical selection. It would thus be interesting to further explore consequences of this framework for assessing the robustness and the evolvability of autocatalytic networks.

We acknowledge J. Unterberger, L. Jullien, W. Liebermeister, P. Gaspard and A. Blokhuis for stimulating discussions. D. L. received support from the grants ANR-11-LABX-0038, ANR-10-IDEX-0001-02.

- 
- [1] P. Schuster, Monatshefte für Chemie-Chemical Monthly **150**, 763 (2019).
- [2] J. C. Xavier, W. Hordijk, S. Kauffman, M. Steel, and W. F. Martin, Proceedings of the Royal Society B: Biological Sciences **287** (2020), 10.1098/rspb.2019.2371.
- [3] W. H. Lin, E. Kussell, L. S. Young, and C. Jacobs-Wagner, Proceedings of the National Academy of Sciences of the United States of America **117**, 27795 (2020).
- [4] A. Roy, D. Goberman, and R. Pugatch, Proceedings of the National Academy of Sciences **118**, e2107829118 (2021).
- [5] S. Ameta, Y. J. Matsubara, N. Chakraborty, S. Krishna, and S. Thutupalli, Life **11**, 308 (2021).
- [6] D. Lancet, R. Zidovetzki, and O. Markovitch, Journal of the Royal Society Interface **15** (2018), 10.1098/rsif.2018.0159.
- [7] E. Schrödinger, *What is Life? The Physical Aspect of the Living Cell* (Cambridge University Press, 1944).
- [8] A. Kolchinsky, arXiv (2021), arXiv:2112.02809.
- [9] R. Pascal, A. Pross, and J. D. Sutherland, Open Biology **3**, 130156 (2013).
- [10] R. G. Endres, Scientific Reports **7**, 1 (2017).
- [11] A. B. George, T. Wang, and S. Maslov, bioRxiv (2022), 10.1101/2022.03.11.483989.
- [12] S. D. Cengio, V. Lecomte, and M. Poletti, arXiv [Preprint] (2022), 10.48550/arxiv.2208.01290.
- [13] F. Avanzini, E. Penocchio, G. Falasco, and M. Esposito, Journal of Chemical Physics **154**, 94114 (2021), arXiv:2012.10375.
- [14] Y. Hirono, T. Okada, H. Miyazaki, and Y. Hidaka, Physical Review Research **3** (2021), 10.1103/PhysRevResearch.3.013175 (2021), arXiv [Preprint]:2102.07687.
- [15] Y. Sughiyama, D. Loutchko, A. Kamimura, and T. J. Kobayashi, Phys. Rev. Res. **4**, 033065 (2022).
- [16] K. Yoshimura and S. Ito, Physical Review Research **3**, 013175 (2021).
- [17] J. D. Orth, I. Thiele, and B. O. Palsson, Nature Biotechnology **28**, 245 (2010).
- [18] D. Fell and A. Cornish-Bowden, *Understanding the control of metabolism*, Vol. 2 (Portland press London, 1997).
- [19] R. Steuer, T. Gross, J. Selbig, and B. Blasius, Proceedings of the National Academy of Sciences of the United States of America **100**, 12286 (2003).
- [20] A. Blokhuis, D. Lacoste, and P. Nghe, Proceedings of the National Academy of Sciences of the United States of America **119**, 10111 (2022).
- [21] J. Unterberger and P. Nghe, Journal of Mathematical Biology **85**, 26 (2022).
- [22] J. L. Andersen, C. Flamm, D. Merkle, and P. F. Stadler, arXiv [Preprint] (2021).
- [23] Z. Peng, K. Paschek, and J. C. Xavier, BioEssays **44**, 1 (2022).
- [24] A. Arya, J. Ray, S. Sharma, R. Cruz Simbron, A. Lozano, H. B. Smith, J. L. Andersen, H. Chen, M. Meringer, and H. J. Cleaves, Chem. Sci. **13**, 4838 (2022).
- [25] A. Wachtel, R. Rao, and M. Esposito, New Journal of Physics **20** (2018), 10.1088/1367-2630/aab5c9, arXiv:1709.06045.
- [26] M. Feinberg, *Foundations of chemical reaction network theory* (Springer, 2019) pp. 26–27.
- [27] R. Rao and M. Esposito, Physical Review X **6** (2016), 10.1103/PhysRevX.6.041064, arXiv:1602.07257.
- [28] M. Poletti and M. Esposito, Journal of Chemical Physics **141** (2014), 10.1063/1.4886396, arXiv:1404.1181.
- [29] M. Pekař, *Progress in Reaction Kinetics and Mechanism*, Vol. 30 (Science Reviews Ltd, 2005) pp. 3–113.
- [30] D. Kondepudi and I. Prigogine, *Modern Thermodynamics* (John Wiley & Sons, Ltd, 2014).
- [31] M. Baiesi and C. Maes, Journal of Physics Communications **2**, 45017 (2018).
- [32] M. Vellela and H. Qian, Journal of the Royal Society Interface **6**, 925 (2009).
- [33] C. N. Hinshelwood, Journal of the Chemical Society , 745 (1952).
- [34] U. Ehrenholz, D. Davidi, E. Reznik, Y. Bar-On, N. Antonovsky, E. Noor, and R. Milo, eLife **6**, 1 (2017).
- [35] E. Noor, A. Bar-Even, A. Flamholz, E. Reznik, W. Liebermeister, and R. Milo, PLoS computational biology **10**, e1003483 (2014).
- [36] J. A. Owen and J. M. Horowitz, Nature Communications **14**, 1280 (2023).
- [37] S. Liang, P. D. L. Rios, and D. M. Busiello, arXiv (2023), 10.48550/arXiv.2212.12074.
- [38] T. De Donder, Mémoires de la Classe des sciences. Académie royale de Belgique. Collection in 8 **9**, 1 (1927).



## Materials and Methods

In the section Materials and Methods below, we introduce some notations for our framework, we detail the kinetics and thermodynamics of CRN, we provide a derivation of the structural constraints and we explain how degradation can be included in the framework. The SI Appendix comprises the following sections: 1) A detailed analysis of Type I network; 2) further details on the stoichiometric analysis of general CRNs; 3) an extension of the framework to non-ideal systems; 4) a study of the thermodynamic bound for generic autocatalytic networks including 3x3 networks but also more general networks and a procedure to reduce the analysis to simpler networks; 5) A study of the bistable Schlögl model and of the Hinshelwood cycle.

### Setup and notation

We assume that the chemical reaction network (CRN) is described by a stoichiometric matrix of the form

$$\nabla = \mathcal{E} \begin{array}{c} \uparrow \\ \left( \begin{array}{c} \nabla^{ex} \\ \vdots \\ \mathbb{S} \\ \vdots \\ \mathbf{0} \end{array} \right) \\ \downarrow \end{array}, \quad (34)$$

$\xleftrightarrow{\mathcal{P}}$

where  $\mathcal{E}$  is the set of all species and  $\mathcal{P}$  is the set of all reactions in the full system. The restriction of  $\nabla$  on  $\mathcal{E}^{ex}$  (denoted  $\nabla^{ex}$ ) describes external species, while  $\mathbb{S}$  is the stoichiometric matrix of autocatalytic species. By assumption, it is a square invertible matrix. Thus, one has  $\mathcal{E} = \mathcal{E}^{ex} \cup \mathcal{Z}$  and  $\mathcal{P} = \mathcal{P}^{ex} \cup \mathcal{R}$ , where  $\mathcal{Z}$  is the set of *autocatalytic species* and  $\mathcal{R}$  is the set of *autocatalytic reactions*. The autocatalytic network is coupled to *external species* in  $\mathcal{E}^{ex}$  which are involved in additional reactions  $\mathcal{P}^{ex}$ . A somewhat similar matrix decomposition has been introduced in Ref. [12] to study geometrical features of non-equilibrium reaction networks.

After chemostatting all the external species, the autocatalytic CRN is still able to reach detailed balance. To see this, one can multiply the matrix  $\nabla$  on its left hand side by the row vector  $(\boldsymbol{\mu}_{ex}, \boldsymbol{\mu})$ , where  $\boldsymbol{\mu}_{ex}$  are the chemical potentials of the external species and  $\boldsymbol{\mu}$  the chemical potentials of the autocatalytic species. This yields

$$\boldsymbol{\mu}_{ex} \cdot (\nabla^{ex})_{\mathcal{R}} + \boldsymbol{\mu} \cdot \mathbb{S} = \mathbf{0}, \quad (35)$$

with  $(\nabla^{ex})_{\mathcal{R}}$  being the restriction of  $\nabla^{ex}$  to the space of autocatalytic reactions  $\mathcal{R}$ . As  $\mathbb{S}$  is non-singular (35) has a unique solution,

$$\boldsymbol{\mu} = -\boldsymbol{\mu}_{ex} \cdot (\nabla^{ex})_{\mathcal{R}} \cdot \mathbb{S}^{-1}, \quad (36)$$

meaning that the autocatalytic CRN is able to reach an equilibrium state even though the additional reactions  $\mathcal{P}^{ex}$  are kept away from equilibrium ( $\boldsymbol{\mu}_{ex} \cdot (\nabla^{ex})_{\mathcal{P}^{ex}} \neq \mathbf{0}$ ).

### Kinetics and thermodynamics of the CRN

We provide here more details on the method to obtain bounds on the global affinity of the network for a general network.

Given the form the fluxes of (21), the corresponding elementary affinities are given by [30, 38]

$$\mathcal{A}_\rho = \ln \left( \frac{j_{+\rho}}{j_{-\rho}} \right) = \ln \left( \frac{k_{+\rho}}{k_{-\rho}} \right) - \sum_{\sigma} S_{\rho}^{\sigma} \ln z_{\sigma}. \quad (37)$$

Consequently, the affinity of the global reaction associated to the elementary mode of production of species  $X$  reads:

$$\mathcal{A} = \sum_{\rho} g_X^{\rho} \mathcal{A}_{\rho} = \sum_{\rho} g_X^{\rho} \ln \left( \frac{k_{+\rho}}{k_{-\rho}} \right) - \sum_{\rho, \sigma} g_X^{\rho} S_{\rho}^{\sigma} \ln z_{\sigma}. \quad (38)$$

Since  $\mathbf{S}^X \cdot \mathbf{g}_X = 1$  and  $\mathbf{S}^Y \cdot \mathbf{g}_X = 0$ , the first term in the right hand side of this equation is the logarithm of the equilibrium constant  $K$ , while the second term is the logarithm of the reaction quotient  $Q$ , so that

$$\mathcal{A} = \ln \left( \frac{K}{Q} \right), \quad (39)$$

as required [30]. It should be emphasized at this stage that because the concentrations of the fuel/food species are absorbed in the kinetic constants,  $K$  is an effective equilibrium constant that includes these concentrations as well.

We expect that in most cases, the stationary global flux will present at least one maximum as the CRNs are being brought out of equilibrium. Indeed, due to the tight coupling condition, the total entropy production rate (EPR) has a simple expression [13, 27, 28]:

$$\Sigma = \sum_{\rho} j_{\rho} \mathcal{A}_{\rho} = \mathcal{J} \mathcal{A}. \quad (40)$$

Note also that the steady-state flow of matter  $I$  introduced in (15) and the global flux  $\mathcal{J}$  cancel each other thanks to (18):

$$\mathcal{J} + I = 0. \quad (41)$$

We now precisely focus on an extremal point where the derivative of the global flux vanishes:  $d_Q \mathcal{J} = 0$ . Due to the tight coupling condition, (19), all reaction fluxes are also at an extremum, thus  $d_Q j_{\rho} = d_Q j_{+\rho} - d_Q j_{-\rho} = 0$  as well. To characterize this configuration, we introduce the log-derivative of the stationary fluxes, which we call  $F_{\pm\rho}$  and which are defined in the main text in (24). These  $F_{\pm\rho}$ s quantify the response of the steady unidirectional rates ( $j_{\pm\rho}$ ) with respect to a change in steady-state values. Because the derivatives of all the fluxes are zero at the extremum  $Q = Q^*$ , we have for each reaction

$$j_{+\rho}^* F_{+\rho}^* = j_{-\rho}^* F_{-\rho}^*. \quad (42)$$

This relation yields a connection between the elementary affinities and the  $F_{\pm\rho}$ s at an extremum of the global flux:

$$e^{\mathcal{A}_{\rho}^*} = \frac{j_{+\rho}^*}{j_{-\rho}^*} = \frac{F_{-\rho}^*}{F_{+\rho}^*}. \quad (43)$$

We observe that the affinities  $\mathcal{A}_{\rho}^*$  do not depend explicitly on kinetic constants. Now, using (43) into the expression  $\mathcal{A} = \sum_{\rho} g_X^{\rho} \mathcal{A}_{\rho}$ , one obtains (26) of the main text. In the next subsection, we explain the derivation of the structural constraints which are analogous to Kirchhoff's laws.

### Structural constraints

The second law of thermodynamics imposes that the global flux is positive for  $Q \in [0, K[$  and negative for  $Q \geq K$  thus,  $Q^*$  lies in  $[0, K[$ , where  $\mathcal{J}(Q^*) > 0$ . Then, because of the tight coupling condition (19), the signs of  $j_{\rho}^*$  and  $g_X^{\rho}$  are the same. Further, if  $g_X^{\rho} > 0$  then  $j_{\rho}^* > 0$  and thus  $\mathcal{A}_{\rho}^* > 0$ ; conversely, if  $g_X^{\rho} < 0$  then  $j_{\rho}^* < 0$ , yielding  $\mathcal{A}_{\rho}^* < 0$ . We are then left with the special and important case where  $g_X^{\rho} = 0$ , which implies again by (19) that  $j_{\rho} = \mathcal{A}_{\rho}^* = 0$ . In that case, the corresponding reaction  $\rho$  is at equilibrium. To summarize :

$$\forall \rho \in \mathcal{R}, \quad g_X^{\rho} \mathcal{A}_{\rho}^* > 0, \quad \text{and} \quad \mathcal{A}_{\rho}^* = 0 \quad \text{when} \quad g_X^{\rho} = 0. \quad (44)$$

Note that these conditions directly translate into additional non-linear constraints on the  $F_{\pm}$ s at the optimum.

Now, let us derive linear constraints acting on  $F_{\pm}$ s, that follow from (42)-(43) and that hold generally even outside the optimum point  $Q = Q^*$ . To do that, let us consider a linear and a branched reaction pathway, as depicted in Fig. 2. In the linear pathway, an arbitrary species  $Z_i$  is transformed into a product species  $Z_{i+1}$  by a reversible and unimolecular reaction  $\rho_i$ , and then  $Z_{i+1}$  undergoes a similar reaction  $\rho_{i+1}$ . In such case, both  $j_{-\rho_i}$  and  $j_{+\rho_{i+1}}$  depend solely on the concentration  $z_{i+1}$  of species  $Z_{i+1}$ . Consequently,

$$F_{-\rho_i} = F_{+\rho_{i+1}}, \quad (45)$$

because both terms are equal to  $d_Q \ln z_{i+1}$ . Similarly, for a branched pathway where a single initial species  $Z_0$  splits through the reaction  $+\rho_0$  into several products  $Z_i$  with multiplicity given by  $S_{-\rho_0}^i$ , (24) leads to:

$$F_{-\rho_0} = \sum_i S_{-\rho_0}^i F_{+\rho_i}. \quad (46)$$

These relations, which take the form of Kirchoff's laws acting on the log-derivatives of the fluxes, can be grouped into a single equation for row vectors  $\mathbf{F}_{\pm}$  which is given in the main text in (25).

The equations (25) define a linear system of the form  $\mathbb{M} \cdot \mathbf{F}_{+} = 0$ , because  $\mathbf{F}_{-}$  can be expressed in terms of  $\mathbf{F}_{+}$  using the affinities (see (43)). Bounds on  $\mathcal{A}^*$  can then be obtained by solving a convex optimization problem in terms of these variables which is complemented by the structural linear constraints given in (25) and by (44).

### Extension to the case of specific degradation

We show here that the bounds derived by considering that an autocatalytic species is chemostatted remain valid when the chemostatting procedure is replaced by a specific degradation of the same species. Let us call  $\mathbf{X}$  the autocatalytic species in question. We can introduce an augmented stoichiometric matrix and an augmented flux vector to take into account the degradation:

$$\mathbb{S}' = \begin{pmatrix} \mathbf{S}^X & -1 \\ \vdots & \\ \mathbf{S}^Y & \mathbf{0} \end{pmatrix}, \quad \mathbf{v} = \begin{pmatrix} \mathbf{j} \\ \kappa f(x) \end{pmatrix}, \quad (47)$$

where  $\kappa$  is non-negative. The degradation rate is described by the function  $f(x)$ , which can be a simple power law  $x^n$  with  $n > 0$ , or a more sophisticated expression, such as a Hill function:

$$f(x) = \frac{x^n}{x^n + K}, \quad (48)$$

in which  $K$  is usually referred to as the apparent dissociation constant. The Hill function is often used to model kinetics involving the fixation of a substrate on macromolecules (such as proteins), and includes the Michaelis-Menten law as a special case (i.e.,  $n = 1$ ). The dynamics of such an extended system obeys

$$d_t \mathbf{z} = \mathbb{S}' \cdot \mathbf{v}. \quad (49)$$

A steady-state of this new system consists of  $\mathbf{v} \in \ker(\mathbb{S}')$ , the latter being spanned by  $\mathbf{g}'_{\mathbf{X}} = (\mathbf{g}_{\mathbf{X}}, 1)^T$ ,

$$\mathbb{S}' \cdot \mathbf{g}'_{\mathbf{X}} = \begin{pmatrix} \mathbf{S}^X \cdot \mathbf{g}_{\mathbf{X}} - 1 \\ \mathbf{S}^Y \cdot \mathbf{g}_{\mathbf{X}} \end{pmatrix} = \mathbf{0}. \quad (50)$$

Consequently, the steady elementary rates associated with (49) are proportional to  $\mathbf{g}'_{\mathbf{X}}$ :

$$\mathbf{j} = \mathcal{J}(\kappa) \mathbf{g}_{\mathbf{X}}. \quad (51)$$

The steady-state rates of the various reactions still follow the law of mass action, but are now parameterized by  $\kappa$ :

$$j_{\pm\rho}(\kappa) = k_{\pm\rho} \prod_{Z_{\sigma} \in \mathcal{Z}} z_{\sigma}(\kappa)^{S_{\pm\rho}^{\sigma}}. \quad (52)$$

Their total derivative with respect to  $\kappa$  is, like before, proportional to the rates:

$$d_{\kappa} j_{\pm\rho} = \partial_{\kappa} \mathbf{z} \cdot \partial_{\mathbf{z}} j_{\pm\rho} = F_{\pm\rho} \cdot j_{\pm\rho}. \quad (53)$$

We thus recover the same expression as before for the log-derivatives  $F_{\pm}$ s,

$$F_{\pm\rho} = \sum_{\sigma} S_{\pm\rho}^{\sigma} d_{\kappa} \ln z_{\sigma}. \quad (54)$$

As a consequence, we also recover the structural constraints (25).

A few words concerning the properties of the global flux are in order. Injecting the tight coupling condition (51) into the steady-state condition and using (50) yields

$$\mathcal{J}(\kappa) = \kappa f(x). \quad (55)$$

We see that the flux necessarily vanishes when  $\kappa = 0$ . This can be seen as the consequence that the system reaches equilibrium in the absence of degradation. Additionally, (55) implies that  $\mathcal{J}(\kappa) \geq 0$ , which allows us to recover the additional constraints discussed in the second section of Materials and Methods.

We now introduce  $\kappa_c \in ]0, +\infty]$ , which is defined as the value of the degradation rate such that  $x(\kappa_c) = 0$ . If  $\kappa_c < +\infty$  then, for any  $\kappa \geq \kappa_c$ ,  $x(\kappa) = 0$  is the only physically acceptable solution, so that (55) implies  $\mathcal{J}(\kappa) = 0$  as well. On the other hand, if  $\kappa_c$  diverges, (55) imposes that

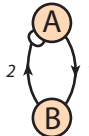
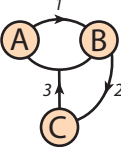
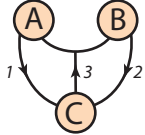
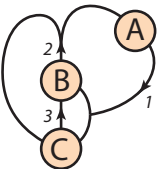
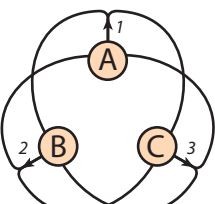
$$x(\kappa)^n \underset{+\infty}{\sim} \kappa^{-\alpha}, \quad \alpha \geq 1. \quad (56)$$

Two qualitatively different situations can be found. If  $\alpha > 1$ , the global flux vanishes for large enough values of  $\kappa$ :  $\mathcal{J}(+\infty) = 0$ . If  $\alpha = 1$ , the global flux converges to a finite non-zero value,  $\mathcal{J}(+\infty) > 0$ . Such systems are similar to those having a non-vanishing global flux when  $Q = 0$  in the chemostatted case. As before, a necessary but not sufficient condition for this to happen is to have a *seed-independent* mode of production.

Because the structural constraints are the same as before, the discussion around the determinant condition and the bound on the five simplest autocatalytic motifs remains valid, with a few subtle differences. Assuming compatible constraints, in the system with one chemostat the maximum of  $\mathcal{J}(Q)$  belongs to  $]0, K[$  ( $Q^* \neq 0$ ), while in the case of specific degradation, the maximum of  $\mathcal{J}(\kappa)$  is attained for a value  $\kappa^* < +\infty$ .

If the constraints are incompatible,  $\mathcal{J}(Q)$  is a decreasing function of  $Q$  with  $Q^* = 0$  when chemostatting (see Fig. 3.B). In the system with specific degradation, we recover this behavior, but in this case the species  $X$  is completely depleted when  $\kappa^* = \kappa_c$ . Furthermore, because the constraints associated to  $\kappa^*$  are incompatible, we know that  $\kappa^*$  is either 0 or  $+\infty$ , where the constraints are not valid because the definition of the  $F_{\pm}$ s do not apply. Since  $\kappa^* = 0$  is the equilibrium state,  $\kappa^* = \kappa_c = +\infty$ , making  $\mathcal{J}(\kappa)$  an increasing function (Fig. 3.C of the main text). Note that the converse is not true: it is possible that the rate converges to a finite non-zero value with  $\kappa^* < +\infty$ .



Motif	$\mathbb{S}$	$\mathbb{S}^{-1}$	Overall equation along $\mathbf{g}_X$	Bound on $\mathcal{A}^*$
 Type I	$\begin{matrix} A & \begin{pmatrix} -1 & 1 \\ 1 & -1 \end{pmatrix} \\ B & \end{matrix}$	$\begin{matrix} 1 & \begin{pmatrix} 1 & 2 \\ 1 & 1 \end{pmatrix} \\ 2 & \end{matrix}$	$A + B \xrightarrow{g_A} 2A + B$  $2A + B \xrightarrow{g_B} 2A + 2B$	$\mathcal{A}^* = \ln 2$  $\mathcal{A}^* \geq \ln 2$
 Type II	$\begin{matrix} A & \begin{pmatrix} -1 & 0 & 1 \\ 1 & -1 & 1 \\ 0 & 1 & -1 \end{pmatrix} \\ B & \\ C & \end{matrix}$	$\begin{matrix} 1 & \begin{pmatrix} 0 & 1 & 1 \\ 1 & 1 & 2 \\ 1 & 1 & 1 \end{pmatrix} \\ 2 & \\ 3 & \end{matrix}$	$B + C \xrightarrow{g_A} A + B + C$  $A + B + C \xrightarrow{g_B} A + 2B + C$  $A + 2B + C \xrightarrow{g_C} A + 2B + 2C$	$\mathcal{A}^* = \ln 2$  $\mathcal{A}^* \geq \ln 2$  $\mathcal{A}^* \geq \ln 2$
 Type III	$\begin{matrix} A & \begin{pmatrix} -1 & 1 & 1 \\ 1 & -1 & 1 \\ 0 & 0 & -1 \end{pmatrix} \\ B & \\ C & \end{matrix}$	$\begin{matrix} 1 & \begin{pmatrix} 1 & 1 & 1 \\ 1 & 0 & 1 \\ 1 & 1 & 0 \end{pmatrix} \\ 2 & \\ 3 & \end{matrix}$	$A + B + C \xrightarrow{g_A} 2A + B + C$  $A + C \xrightarrow{g_B} A + B + C$  $A + B \xrightarrow{g_C} A + B + C$	$\mathcal{A}^* \geq \ln 2$  $\mathcal{A}^* \geq \ln 2$  $\mathcal{A}^* \geq \ln 2$
 Type IV	$\begin{matrix} A & \begin{pmatrix} -1 & 1 & 0 \\ 1 & -1 & 1 \\ 1 & 1 & -1 \end{pmatrix} \\ B & \\ C & \end{matrix}$	$\begin{matrix} 1 & \begin{pmatrix} 0 & 1/2 & 1/2 \\ 1 & 1/2 & 1/2 \\ 1 & 1 & 0 \end{pmatrix} \\ 2 & \\ 3 & \end{matrix}$	$B + C \xrightarrow{g_A} A + B + C$  $\frac{1}{2}A + \frac{1}{2}B + C \xrightarrow{g_B} \frac{1}{2}A + \frac{3}{2}B + C$  $\frac{1}{2}A + \frac{1}{2}B \xrightarrow{g_C} \frac{1}{2}A + \frac{1}{2}B + C$	$\mathcal{A}^* \geq \ln 3$  $\mathcal{A}^* \geq \frac{\ln 3}{2}$  $\mathcal{A}^* \geq \frac{\ln 3}{2}$
 Type V	$\begin{matrix} A & \begin{pmatrix} -1 & 1 & 1 \\ 1 & -1 & 1 \\ 1 & 1 & -1 \end{pmatrix} \\ B & \\ C & \end{matrix}$	$\begin{matrix} 1 & \begin{pmatrix} 0 & 1/2 & 1/2 \\ 1/2 & 0 & 1/2 \\ 1/2 & 1/2 & 0 \end{pmatrix} \\ 2 & \\ 3 & \end{matrix}$	$\frac{1}{2}B + \frac{1}{2}C \xrightarrow{g_A} A + \frac{1}{2}B + \frac{1}{2}C$  $\frac{1}{2}A + \frac{1}{2}C \xrightarrow{g_B} \frac{1}{2}A + B + \frac{1}{2}C$  $\frac{1}{2}A + \frac{1}{2}B \xrightarrow{g_C} \frac{1}{2}A + \frac{1}{2}B + C$	$\mathcal{A}^* \geq \ln 3$  $\mathcal{A}^* \geq \ln 3$  $\mathcal{A}^* \geq \ln 3$

**Table I:** Bound on the chemical affinities at the extremum of the macroscopic flux for the five most simple autocatalytic motif derived in [20]. The modes of production that are *seed-dependent* are highlighted in green and the *seed-independent* mode of production are highlighted in blue, each of them obey the two principles of the main text on the minimal cost needed to sustain the production of the X-species. With the exception of Type IV when species A is chemostatted, the principles provide the tightest bound, i.e. saturable for a certain limited choice of kinetic constants and observed numerically.

# Supporting Information for

## Structural constraints limit the regime of optimal flux in autocatalytic reaction networks

### TYPE I NETWORK WITH SPECIES B CHEMOSTATTED

As claimed in the main text, the introductory example can be solved explicitly in the case  $\alpha = 1$ ,  $\beta = 2$ ,



When species B is chemostatted, the steady-state concentration of A,  $a$ , is the root of a second-order polynomial:

$$\text{d}_t a = 0 = 2k_{+2}b - 2k_{-2}wa^2 + k_{-1}b - k_{+1}fa. \quad (58)$$

The latter is easily solved and leads to the following expression for the macroscopic current:

$$\mathcal{J} = k_{+2}b - \frac{(k_{+1}f)^2}{16k_{-2}w} \cdot \left( 1 - \sqrt{1 + \frac{8k_{-2}(2k_{+2} + k_{-1})bw}{k_{+1}^2 f^2}} \right)^2. \quad (59)$$

$\mathcal{J}$  shares the same sign as the chemical affinity and has an extremum when

$$\frac{b^* w}{f^2} = \frac{1}{2} \frac{k_{+1}^2 k_{+2}}{k_{-1}^2 k_{-2}} \frac{k_{+2} + k_{-1}}{2k_{+2} + k_{-1}}. \quad (60)$$

At this point, the reaction quotient is given by

$$Q^* = \frac{K}{2} \frac{k_{+2} + k_{-1}}{2k_{+2} + k_{-1}} \leq \frac{K}{2}. \quad (61)$$

Thus, when B is chemostated the optimal affinity is bounded by a simple rate-independent constant:

$$\mathcal{A}^* \geq \ln 2. \quad (62)$$

When one makes no assumption on  $\alpha$ ,  $\beta$  (with  $0 < \alpha < \beta$ ), the steady-state (58) becomes a higher-order polynomial. Computing the roots of such polynomials is in general difficult. This illustrates the need of a more tractable procedure to extract the bound on the chemical affinity, which would not rely on the explicit solutions of the steady-state problem as explained in the main text.

### STOICHIOMETRIC ANALYSIS OF OPEN INVERTIBLE CHEMICAL REACTION NETWORKS

#### General properties of the autocatalytic CRN

We assume that external species are externally controlled (chemostatted) and include their concentrations in the rate constants of the reactions. For any  $\rho \in \mathcal{R}$ :

$$\sum_{\sigma} S_{+\rho}^{\sigma} Z_{\sigma} \xrightleftharpoons[k_{-\rho}]{k_{+\rho}} \sum_{\sigma} S_{-\rho}^{\sigma} Z_{\sigma}, \quad (63)$$

with the autocatalytic species  $Z_{\sigma} \in \mathcal{Z}$  being indexed by  $\sigma$ . The  $k_{\pm\rho}$ s are the (effective) kinetic rate constants and the coefficients  $S_{+\rho}^{\sigma}$  (resp.  $S_{-\rho}^{\sigma}$ ) encode the molecularities of the product for the forward (resp. reverse) transition  $+\rho$  (resp.  $-\rho$ ), such that:

$$\mathbb{S} = \mathbb{S}_{-} - \mathbb{S}_{+}. \quad (64)$$

The deterministic dynamics of the full CRN is given by

$$d_t \mathbf{e} = \nabla^{ex} \cdot \mathbf{v} + \mathbf{I}^{ex} = 0 \quad (65)$$

$$d_t \mathbf{z} = \mathbb{S} \cdot \mathbf{j}, \quad (66)$$

where  $\mathbf{e}$  are the concentrations of the external species,  $\mathbf{v}$  are the net fluxes of all the reactions ( $\mathcal{P}$ ),  $\mathbf{j}$  its restriction on the autocatalytic reaction ( $\mathcal{R}$ ):  $\mathbf{j} \equiv \mathbf{v}^{\mathcal{R}}$  and  $\mathbf{I}^{ex}$  the external flux.

We call respectively  $\mathcal{C}$  and  $\mathcal{L}$  the set of cycles and the set of conservation laws associated to  $\nabla$  (*i.e.* its kernel and its cokernel). Similarly, we refer to  $\tilde{\mathcal{C}}$  and  $\tilde{\mathcal{L}}$  respectively as the cycles and the conservation laws of  $\nabla^{\mathcal{Z}}$ , the restriction of  $\nabla$  on the set of autocatalytic species. The rank-nullity theorem links the number of external species,  $|\mathcal{E}^{ex}|$ , to the number of emergent cycles (cycles in  $\tilde{\mathcal{C}}$  but not in  $\mathcal{C}$ ),  $|\tilde{\mathcal{C}}| - |\mathcal{C}|$ , and the number of broken conservation laws,  $|\mathcal{L}| - |\tilde{\mathcal{L}}|$ :

$$|\mathcal{E}^{ex}| = |\tilde{\mathcal{C}}| - |\mathcal{C}| + |\mathcal{L}| - |\tilde{\mathcal{L}}|. \quad (67)$$

Additionally, the non-singularity of  $\mathbb{S}$  dictates that the only steady state for the autocatalytic dynamics is the equilibrium configuration  $\mathbf{j}_{eq} = \mathbf{0}$ . Nonetheless, depending on how the external species are coupled to the autocatalytic CRN, two situations can emerge, impacting (67).

*Case  $\mathcal{P}^{ex} = \emptyset$*  If the external species are not involved in any additional reaction, the full stoichiometric matrix simplifies to

$$\nabla = \mathcal{E} \begin{array}{c} \uparrow \left( \begin{array}{c} \nabla^{ex} \\ \cdots \\ \mathbb{S} \end{array} \right) \\ \downarrow \\ \longleftrightarrow \\ \mathcal{R} \end{array}, \quad (68)$$

where we see that the set of autocatalytic reaction  $\mathcal{R}$  is shared by  $\mathbb{S}$  and  $\nabla^{ex}$ . In that case, the matrix encoding the properties of the open CRN simplifies as well:  $\nabla^{\mathcal{Z}} = \mathbb{S}$ . Hence the non-singularity of  $\mathbb{S}$  implies that:

1.  $\tilde{\mathcal{C}} = \mathcal{C} = \emptyset$ , no emergent cycle appears after chemostating the external species,
2.  $\tilde{\mathcal{L}} = \emptyset$ , the open CRN has no conservation law.

The absence of conservation in  $\mathbb{S}$  is a hallmark of autocatalysis. However, chemical consistency enforces (at least) the conservation of the total mass when the full network is closed ( $\mathbf{I}^{ex} = \mathbf{0}$ ) and as consequence,  $\mathcal{L}$  is never empty. It follows from (67) that the number of conserved quantities in the full network is equal to the number of external species,  $|\mathcal{L}| = |\mathcal{E}^{ex}|$ . Thus, all the conservation laws are broken once the species in  $\mathcal{E}^{ex}$  are chemostatted, which means that no emergent cycle emerges. Using the classification of Anvizini *et al.* [13], in that case the external species are *potential species* that are not able to break detailed balance. As a consequence, for any values of the concentrations of external species, nothing prevents the autocatalytic CRN from reaching equilibrium.

*Case  $\mathcal{P}^{ex} \neq \emptyset$*  There is no specific reason to assume that external species are not involved in additional reactions (for example ATP hydrolysis in the context of metabolic networks). After clamping the external species, the stoichiometric matrix of the open system is:

$$\nabla^{\mathcal{Z}} \equiv \mathcal{Z} \begin{array}{c} \uparrow \left( \begin{array}{c} \mathbb{S} \\ \vdots \\ \mathbf{0} \end{array} \right) \\ \downarrow \\ \longleftrightarrow \\ \mathcal{P} \end{array}, \quad (69)$$

which has  $|\mathcal{P}^{ex}|$  independent (emergent) cycles. Therefore, still following the nomenclature proposed by Anvizini, there will be  $|\mathcal{P}^{ex}|$  *force species*, which can possibly break detailed balance.

Because the autocatalytic species are not involved in reactions  $\mathcal{P}^{ex}$ , this subset of reactions can remain out of equilibrium while the autocatalytic CRN is still able reach detailed balance. However, as seen in the first section of the Material and Methods of the main text, the autocatalytic CRN is able to reach an equilibrium state nonetheless.

## Modes of production of the network

As we just saw, chemostating the external species is not sufficient to maintain autocatalysis in a steady-state because the autocatalytic CRN will reach equilibrium. Consequently, maintaining autocatalysis steadily requires that the concentration of (at least) one of the autocatalytic species be chemostatted as well. We will denote this chemostatted autocatalytic species with an  $X$ , which thus has a constant concentration  $x$ . As in the main text, the  $|\mathcal{Z}| - 1$  non-chemostatted autocatalytic species are called the  $Y$ -species, and their concentration are grouped in  $\mathbf{y}$ .

Taking this into account in (66) leads to Eqs. (15)-(16) of the main text for the dynamics of the out-of-equilibrium autocatalytic CRN. The inverse of  $\mathbb{S}$  splits accordingly:

$$\mathbb{S}^{-1} = (\mathbf{g}_X, \mathbb{G}_Y), \quad (70)$$

where we stacked in  $\mathbb{G}_Y$  the columns of  $\mathbb{S}^{-1}$  associated to the  $Y$  species. Consequently,

$$\mathbb{S} \cdot \mathbb{S}^{-1} = \begin{pmatrix} \mathbf{S}^X \cdot \mathbf{g}_X & \mathbf{S}^X \cdot \mathbb{G}_Y \\ \vdots & \vdots \\ \mathbb{S}^Y \cdot \mathbf{g}_X & \mathbb{S}^Y \cdot \mathbb{G}_Y \end{pmatrix} = \text{Id.}, \quad (71)$$

in which  $\mathbf{S}^X$  and  $\mathbb{S}^Y$  were respectively defined as the row vector of  $\mathbb{S}$  associated to the chemostatted autocatalytic species and the restriction on the  $Y$ -species of  $\mathbb{S}$ . This leads to:

$$\mathbf{S}^X \cdot \mathbf{g}_X = 1 \quad (72)$$

$$\mathbb{S}^Y \cdot \mathbf{g}_X = \mathbf{0}. \quad (73)$$

These two equations quantify the two properties of the *elementary mode of production* of species  $X$ :  $\mathbf{g}_X$  is reaction pathway that produces one extra unit of species  $X$  (72) letting the  $Y$ -species unchanged ((73)). Additionally, from (73) and the rank-nullity theorem using  $\tilde{\mathcal{C}} = \emptyset$ , we have  $\ker(\mathbb{S}^Y) = \text{span}(\mathbf{g}_X)$ .

*Seed-dependency of  $\mathbf{g}_X$*  Let us note  $\mathcal{R}_X \subset \mathcal{R}$  the subset of autocatalytic reactions having species  $X$  as reactant, note that if  $\rho$  has  $X$  as product then  $-\rho \in \mathcal{R}_X$ . The sign of the restriction of  $\mathbf{g}_X$  to  $\mathcal{R}_X$ ,  $\mathbf{g}_X^{\mathcal{R}_X}$ , allows to know if  $\mathbf{g}_X$  is a *seed-dependent* or a *seed-independent* mode of production. If  $\mathbf{g}_X^{\mathcal{R}_X}$  has at least one positive component,  $X$  is consumed by, at least, one reaction in the overall reaction consequently, the mode of production will be *seed-dependent*. Conversely, if  $\mathbf{g}_X^{\mathcal{R}_X} \leq 0$  (component-wise),  $X$  will not be present in the reactant side in the overall equation then  $\mathbf{g}_X$  will be *seed-independent*.

With that we can show that, along a seed-dependent mode of production, the macroscopic current is necessarily vanishing at zero. Indeed, if  $\mathbf{g}_X$  is *seed-dependent* there exists  $\rho \in \mathcal{R}_X$  such that,  $g_X^\rho > 0$ . Hence, for all  $Q \in [0, K]$ ,  $j_\rho(Q) \geq 0$ . In addition,  $j_\rho(0) = -j_{-\rho}(0) \leq 0$ . Combining this with the previous inequality, we get  $j_\rho(0) = 0$ . Because  $\mathcal{J}(Q) = (g_X^\rho)^{-1} j_\rho(Q)$ , we obtain that  $\mathcal{J}(0) = 0$ .

*The renormalized mode of production* There is no guarantee that the stoichiometric coefficients of the global chemical equation associated with  $\mathbf{g}_X$  are all integers. Formally, this is not a problem and it is possible to carry all the computations for the bounds with rational numbers. However, we need these coefficients to be integers in order to interpret the bounds like we did in the main text. Remembering that  $\mathbf{g}_X$  comes from  $\mathbb{S}^{-1}$ , and because  $\mathbb{S}$  is a matrix of integers, we note that it is possible to multiply  $\mathbb{S}^{-1}$  by some positive integer so that the result contains only integers. It is particularly interesting to consider  $n \in \mathbb{N}^*$ , the smallest positive integer such that  $\hat{\mathbf{g}}_X \equiv n \mathbf{g}_X$  is integer-valued. Similarly, along this new pathway the overall affinity is  $\hat{\mathcal{A}} = n \mathcal{A}$ .

As a consequence, when we wrote the overall equation of a *seed dependent/independent* at steady-state as in the form of Eqs. (28)-(31) of the main text, we implicitly place ourselves along  $\hat{\mathbf{g}}_X$  instead of  $\mathbf{g}_X$ .

## REGIME OF MAXIMUM GLOBAL STATIONARY FLUX FOR NON-IDEAL SYSTEMS

### Structural constraints

At the steady state, the concentrations of the  $Y$ -species relax to their  $Q$ -dependent values  $\mathbf{y}(Q)$ ,  $Q$  stands for the concentration of species  $X$ . Isolating the concentration of the chemostatted species in the steady currents, we can



write:

$$j_{\pm\rho}(Q) = k_{\pm\rho} Q^{S_{\pm\rho}^X} \prod_{Y_\sigma \in Y} y_\sigma(Q)^{(S^Y)_{\pm\rho}^\sigma}. \quad (74)$$

The total derivative of (74) reads

$$d_Q j_{\pm\rho} = \partial_Q j_{\pm\rho} + d_Q \mathbf{y} \cdot \partial_{\mathbf{y}} j_{\pm\rho} = \left( \frac{S_{\pm\rho}^X}{Q} + \sum_{Y_\sigma \in Y} (S^Y)_{\pm\rho}^\sigma \frac{d_Q y_\sigma}{y_\sigma} \right) j_{\pm\rho}. \quad (75)$$

Consequently, the  $F_{\pm\rho}$ s are defined as

$$\mathbf{F}_\pm = d_Q \boldsymbol{\mu} \cdot \mathbb{S}_\pm. \quad (76)$$

where  $\boldsymbol{\mu}$  is a vector of chemical potentials. This expression remains valid for  $Q \in \mathbb{R}^*$ . This will play a central role when analyzing the case of a diverging lower bound. From (76), we interpret the  $\mathbf{F}_\pm$ s as coefficients quantifying the response of the stationary chemical potentials to a perturbation of  $Q$ .

In what follows, we assume that the matrix  $\mathbb{S}_+$  is invertible. We interpret this assumption as the property that the reactions in the autocatalytic network are reactant-independent, in the sense that it not possible to recover the reactants of any reaction by a linear combination of the reactants of other reactions. This means that a given a set of reactants can experience only one reaction together. Under such conditions,  $\mathbf{F}_+$  is directly related to the derivative of the chemical potential through:  $d_Q \boldsymbol{\mu} = \mathbf{F}_+ \cdot \mathbb{S}_+^{-1}$ , yielding the general relation

$$\mathbf{F}_- = \mathbf{F}_+ \cdot (\mathbb{S}_+^{-1} \cdot \mathbb{S}_-). \quad (77)$$

We expect this hypothesis to hold for a wide variety of chemical networks. As an illustration of this, we note that after chemostatting the external species we are often left with a square autocatalytic cycle, in which each reaction consumes only one kind of autocatalytic species (and possibly many external ones) to form other autocatalytic species. Since we assumed the autonomy of the autocatalytic network, each autocatalytic species  $Z_\sigma$  is uniquely associated to one reaction  $\rho_\sigma$ . This species-specific reaction consumes a single unit of  $Z_\sigma$ , and thus  $\mathbb{S}_+ = \text{Id}$ , which is indeed invertible. In that case,  $\mathbf{F}_+ = d_Q \boldsymbol{\mu}$  and we can plug it into the expression of  $\mathbf{F}_-$  to recover Eq. (36) of the main text:  $\mathbf{F}_- = \mathbf{F}_+ \cdot \mathbb{S}_-$ .

### Extension to non-ideal systems

Our derivation of the structural relations (77) seems to be conditional on the use of mass-action laws, and thus on the assumption of ideality. However, we can extend (77) to the case of non-ideal mixtures. In such case, one should take include *activity coefficients*  $\gamma_\sigma$  in the definition of chemical potentials:  $\mu_\sigma = \mu_\sigma^0 + \ln(\gamma_\sigma z_\sigma)$ . Because of thermodynamic consistency, it is expected that the non-ideal microscopic currents,  $j_{\pm\rho}$ , obey the de Donder relation

$$\frac{j_{+\rho}}{j_{-\rho}} = \exp \left( - \sum_{\sigma} \mu_{\sigma} S_{\rho}^{\sigma} \right) = e^{\mathcal{A}}. \quad (78)$$

The reaction rates can thus always be written as

$$j_{+\rho} = \frac{1}{\tau_{\rho}} \exp \left( \sum_{\sigma} \mu_{\sigma} S_{+\rho}^{\sigma} \right), \quad j_{-\rho} = \frac{1}{\tau_{\rho}} \exp \left( \sum_{\sigma} \mu_{\sigma} S_{-\rho}^{\sigma} \right), \quad (79)$$

where  $\tau_{\rho}$  is a characteristic timescale of the reaction.

We must recover the ideal kinetic laws when  $\gamma_{\sigma} = 1$ , which implies that in such case

$$k_{\pm\rho} = \frac{1}{\tau_{\rho}} \exp \left( \sum_{\sigma} \mu_{\sigma}^0 S_{\pm\rho}^{\sigma} \right). \quad (80)$$

Assuming this parametrization to hold in the presence of intermolecular interactions, we note that the derivative of the steady unidirectional flows with respect to  $Q$  becomes

$$d_Q j_{\pm\rho} = \left( \sum_{\sigma} d_Q \mu_{\sigma} S_{\pm\rho}^{\sigma} \right) \frac{1}{\tau_{\rho}} \exp \left( \sum_{\sigma} \mu_{\sigma} S_{\pm\rho}^{\sigma} \right) = F_{\pm\rho} j_{\pm\rho}, \quad (81)$$

with  $F_{\pm\rho} = d_Q \boldsymbol{\mu} \cdot \mathbf{S}_{\pm\rho}$ , as in (76). We thus recover the same structural relations as before, but with a generalized definition of the response coefficients  $F_{\pm\rho}$ . Note that the expression we use for the kinetic rate constants (80) amounts to assuming that the  $\tau_\rho$ s are constant. Having concentration-dependent time scales (and thus, concentration-dependent rate constants) is a possibility that would not affect (78). However, this would impact the derivative of the currents  $j_{\pm\rho}$  and would strongly modify the structural constraints.

## BOUND ON THE THERMODYNAMIC AFFINITY FOR GENERIC AUTOCATALYTIC NETWORKS

### Bound for 3×3 autocatalytic networks

Here, we study generic 3×3 autocatalytic networks because this covers all the simplest autocatalytic cores found in [20] (except Type I, which is 2×2). For an arbitrary 3×3 network,  $\mathbb{S}_-$  is a 3×3 matrix of positive coefficients of the following form:

$$\mathbb{S}_- = \begin{pmatrix} 0 & \alpha & \beta \\ \gamma & 0 & \delta \\ \varepsilon & \zeta & 0 \end{pmatrix}. \quad (82)$$

Assuming that  $\mathbb{S}_+$  is the identity matrix (which is the case for all the autocatalytic cores found in [20]), the structural constraints Eq. (25) of the main text can be written as  $\mathbf{F}_+ \cdot \mathbb{M} = 0$ , with

$$\mathbb{M} = \begin{pmatrix} e^{\mathcal{A}_1^*} & -\alpha & -\beta \\ -\gamma & e^{\mathcal{A}_2^*} & -\delta \\ -\varepsilon & -\zeta & e^{\mathcal{A}_3^*} \end{pmatrix}. \quad (83)$$

We are looking for non-trivial solutions  $\mathbf{F}_+ \neq \mathbf{0}$ . As a result, we further enforce  $\det(\mathbb{M}) = 0$ . This yields:

$$e^{\mathcal{A}_1^* + \mathcal{A}_2^* + \mathcal{A}_3^*} = \delta \zeta e^{\mathcal{A}_1^*} + \beta \varepsilon e^{\mathcal{A}_2^*} + \alpha \gamma e^{\mathcal{A}_3^*} + \beta \gamma \zeta + \alpha \delta \varepsilon. \quad (84)$$

Since the elements of  $\mathbb{S}$  are natural integers,  $\mathbb{S}^{-1}$  is a matrix of rational numbers. As a consequence, there exists some *minimal*  $n \in \mathbb{N}^*$  such that  $\hat{\mathbf{g}}_{\mathbf{X}} = n \mathbf{g}_{\mathbf{X}}$  is an integer-valued vector. We can thus define  $\hat{\mathcal{A}} = \sum_{\rho} \hat{g}_{\mathbf{X}}^{\rho} \mathcal{A}_{\rho}^* = n \mathcal{A}^*$ . If  $\mathbf{g}_{\mathbf{X}} \geq 0$  (component-wise), so is  $\hat{\mathbf{g}}_{\mathbf{X}}$ , and we can easily find a lower bound for the right-hand side of (84):

$$e^{\hat{\mathcal{A}}} \geq e^{\mathcal{A}_1^* + \mathcal{A}_2^* + \mathcal{A}_3^*} \geq \delta \zeta + \beta \varepsilon + \alpha \gamma + \beta \gamma \zeta + \alpha \delta \varepsilon, \quad (85)$$

because  $g_{\mathbf{X}}^{\rho} \geq 0$  implies  $\exp(\mathcal{A}_{\rho}^*) \geq 1$ . Consequently, we obtain the following general form for the bound of  $\mathcal{A}^*$ :

$$\mathcal{A}^* \geq \frac{1}{n} \ln(\delta \zeta + \beta \varepsilon + \alpha \gamma + \beta \gamma \zeta + \alpha \delta \varepsilon). \quad (86)$$

Let us assume for example that  $g_{\mathbf{X}}^1 \leq 0$  and  $g_{\mathbf{X}}^2, g_{\mathbf{X}}^3 \geq 0$ . Then,

$$0 < \exp(\mathcal{A}_1^*) \leq 1, \quad \exp(\mathcal{A}_2^*) \geq 1, \quad \exp(\mathcal{A}_3^*) \geq 1. \quad (87)$$

In such case, the right-hand side of (84) cannot be lower-bounded directly. Nevertheless, multiplying (84) by  $\exp(-2\mathcal{A}_1^*)$  gives:

$$\begin{aligned} e^{-\mathcal{A}_1^* + \mathcal{A}_2^* + \mathcal{A}_3^*} &= \delta \zeta e^{-\mathcal{A}_1^*} + \beta \varepsilon e^{\mathcal{A}_2^* - 2\mathcal{A}_1^*} + \alpha \gamma e^{\mathcal{A}_3^* - 2\mathcal{A}_1^*} \\ &\quad + e^{-2\mathcal{A}_1^*} (\beta \gamma \zeta + \alpha \delta \varepsilon). \end{aligned} \quad (88)$$

Since  $\exp(-\mathcal{A}_1^*) \geq 1$ , we recover (86). Generally speaking, the same procedure can be carried out when two arbitrary components of  $\mathbf{g}_{\mathbf{X}}$  are negative. In this way, we get an equality for  $\exp\left(\sum_{\rho} \text{sgn}(g_{\mathbf{X}}^{\rho}) \mathcal{A}_{\rho}^*\right)$ , which reads

$$e^{\hat{\mathcal{A}}} \geq \exp\left(\sum_{\rho} \text{sgn}(g_{\mathbf{X}}^{\rho}) \mathcal{A}_{\rho}^*\right) \geq \delta \zeta + \beta \varepsilon + \alpha \gamma + \beta \gamma \zeta + \alpha \delta \varepsilon. \quad (89)$$

Note that the bound we get from enforcing  $\det(\mathbb{M}) = 0$  may not always be reachable asymptotically for some choice of the kinetic parameters. In fact, a tighter bound can be obtained by incorporating the structural relations (Eq. (25) of the main text) in (84), as shown below for the derivation of the bound for Type V networks and for the Hinshelwood cycle.

### Extension of the method beyond the 3×3 case

A relation similar to (89) can be derived for an arbitrary 4×4 network. For larger matrices, the method based on the determinant will in general not provide a simple inequality involving the overall affinity. This is because terms of opposite sign can appear in the determinant of  $\mathbb{M}$ , preventing us from writing an equality between  $\exp(\hat{\mathcal{A}})$  and a sum of positive terms that can easily be bounded.

Due to the sparsity of  $\mathbb{S}_-$  for large networks, the determinant condition still works for a broad class of networks beyond the 4×4 case. In particular if, upon re-arranging the rows and columns,  $\mathbb{S}_-$  can be written:

$$\mathbb{S}_- = \begin{pmatrix} 0 & 0 & \cdots & 0 & S_{-N}^1 \\ S_{-1}^2 & \ddots & \ddots & \ddots & 0 \\ \vdots & \ddots & 0 & \ddots & \vdots \\ \vdots & \ddots & \ddots & 0 & 0 \\ S_{-1}^N & \cdots & S_{-(N-1)}^N & 0 & 0 \end{pmatrix}, \quad (90)$$

with  $S_{-N}^1 > 0$ , then the method we presented in Materials and Methods can be generalized to any  $N$ . The form (90) describes a network without *back-branches*, defined as a reaction that has products *upstream* in the network (see Definition 5 in the Supplementary Information of [20]). Assuming that  $\mathbb{S}_-$  indeed satisfies (90), we can expand the first row of  $\mathbb{M} = \text{Diag}(e^{\mathcal{A}_1^*}, \dots, e^{\mathcal{A}_N^*}) - \mathbb{S}_-$  as follows:

$$\det(\mathbb{M}) = e^{\mathcal{A}_1^*} \underbrace{\begin{vmatrix} e^{\mathcal{A}_2^*} & 0 & \cdots & 0 \\ -S_{-2}^3 & \ddots & \ddots & \vdots \\ \vdots & \ddots & 0 & \vdots \\ -S_{-2}^N & \cdots & -S_{-(N-1)}^N & e^{\mathcal{A}_N^*} \end{vmatrix}}_{\text{(I)}} + (-1)^{N+1} (-S_{-N}^1) \underbrace{\begin{vmatrix} -S_{-1}^2 & e^{\mathcal{A}_2^*} & 0 & \cdots & 0 \\ -S_{-1}^3 & -S_{-2}^3 & \ddots & \ddots & \vdots \\ \vdots & \vdots & \ddots & 0 & \vdots \\ -S_{-1}^N & -S_{-2}^N & \cdots & -S_{-(N-1)}^N & e^{\mathcal{A}_{N-1}^*} \end{vmatrix}}_{\text{(II)}}. \quad (91)$$

The first term (I) is the determinant of a diagonal matrix, which is given by the product of its diagonal entries. The second term (II) can be written as

$$\text{(II)} = (-1)^{N-1} \sum_i a_i(\mathbb{S}_-) \prod_j (e^{\mathcal{A}_j^*})^{\alpha_{ij}}, \quad (92)$$

where the coefficients  $a_i(\mathbb{S}_-)$  are positive and depend uniquely on the coefficient in  $\mathbb{S}_-$ ,  $\alpha_{ij}$  is either 0 or 1, and  $(-1)^{N-1}$  is the sign of (II). We can prove property (92) by induction from determinants having the same shape as (II): a negative lower triangular part, and zeros everywhere else except on the first upper diagonal. Denoting  $\Delta_N$  the determinant of an  $N \times N$  matrix of this type, we find for the  $2 \times 2$  case

$$\Delta_2 = \begin{vmatrix} -S_{-1}^2 & e^{\mathcal{A}_2^*} \\ -S_{-1}^3 & -S_{-2}^3 \end{vmatrix} = S_{-1}^2 S_{-2}^3 + S_{-1}^3 e^{\mathcal{A}_2^*}. \quad (93)$$

Assuming (92) to be true for  $N-1$  (with  $N \geq 3$ ) gives

$$\Delta_N = \begin{vmatrix} -S_{-1}^2 & e^{\mathcal{A}_2^*} & 0 & \cdots & 0 \\ -S_{-1}^3 & -S_{-2}^3 & \ddots & \ddots & \vdots \\ \vdots & \vdots & \ddots & 0 & \vdots \\ \vdots & \vdots & \ddots & \ddots & e^{\mathcal{A}_N^*} \\ -S_{-1}^{N+1} & -S_{-2}^{N+1} & \cdots & -S_{-N}^{N+1} & \end{vmatrix} \quad (94)$$

$$= (-S_{-1}^2) \cdot \underbrace{\begin{vmatrix} -S_{-2}^3 & e^{\mathcal{A}_3^*} & 0 & \cdots & 0 \\ -S_{-2}^4 & -S_{-3}^4 & \ddots & \ddots & \vdots \\ \vdots & \vdots & \ddots & 0 & \vdots \\ -S_{-2}^{N+1} & -S_{-3}^{N+1} & \cdots & -S_{-N}^{N+1} & \end{vmatrix}}_{\Delta_{N-1}} - e^{\mathcal{A}_2^*} \cdot \underbrace{\begin{vmatrix} -S_{-1}^3 & e^{\mathcal{A}_3^*} & 0 & \cdots & 0 \\ -S_{-1}^4 & -S_{-2}^4 & \ddots & \ddots & \vdots \\ \vdots & \vdots & \ddots & 0 & \vdots \\ -S_{-1}^{N+1} & -S_{-2}^{N+1} & \cdots & -S_{-N}^{N+1} & \end{vmatrix}}_{\Delta'_{N-1}}. \quad (95)$$

The two determinants  $\Delta_{N-1}$  and  $\Delta'_{N-1}$  obey (92), hence factorizing the  $(-1)$  in (95) yields:  $\text{sgn}(\Delta_N) = (-1)^N$ . We are then left with a sum of products of coefficients in  $\mathbb{S}_-$  (which are positive) and of the  $e^{\mathcal{A}_i^*}$ s. In addition, each  $e^{\mathcal{A}_i^*}$  appear, at most once in each term of the sum because they are present at most once in the determinants  $\Delta_{N-1}$  and  $\Delta'_{N-1}$ . This completes the proof of the property (92)

Enforcing  $\det(\mathbb{M}) = 0$  yields a relation similar to Eq. (55) in the main text for the  $3 \times 3$  case:

$$\exp\left(\sum_{\rho} \mathcal{A}_{\rho}^*\right) = S_{-N}^1 \sum_i a_i(\mathbb{S}_-) \prod_j (e^{\mathcal{A}_j^*})^{\alpha_{ij}}. \quad (96)$$

This equation provides us with a bound on  $\hat{\mathcal{A}} = n \mathcal{A}^*$  (where again,  $n$  is the lowest positive integer that makes the product  $n \mathbf{g}_X$  also an integer):

$$e^{n \mathcal{A}^*} \geq S_{-N}^1 \sum_i a_i(\mathbb{S}_-). \quad (97)$$

### Case of networks with only one branched reaction

From (90), we can derive a simple expression for the lower bound of the affinity for a network containing only one branching reaction with  $\mathbf{p} \geq 2$  products. In that case, we can write

$$\mathbb{S}_- = \begin{pmatrix} 0 & 0 & \dots & 0 & 1 \\ S_{-1}^2 & \ddots & & & 0 \\ S_{-1}^3 & 1 & \ddots & & \vdots \\ \vdots & 0 & \ddots & \ddots & 0 \\ S_{-1}^N & 0 & \dots & 0 & 1 & 0 \end{pmatrix}, \quad (98)$$

with  $\sum_{i=2}^N S_{-1}^i = \mathbf{p}$ . Upon expanding the first row of  $\mathbb{M}$ , we now find

$$\det(\mathbb{M}) = \exp\left(\sum_{\rho} \mathcal{A}_{\rho}^*\right) + (-1)^{N+2} \underbrace{\begin{vmatrix} -S_{-1}^2 & e^{\mathcal{A}_2^*} & 0 & \dots & 0 \\ -S_{-1}^3 & -1 & \ddots & & \vdots \\ \vdots & 0 & \ddots & \ddots & 0 \\ -S_{-1}^N & 0 & \dots & 0 & -1 \end{vmatrix}}_{\Delta_N^2}. \quad (99)$$

Moreover, we have the recurrence relation  $\Delta_N^i = (-1)^{N-i+1} S_{-1}^i - e^{\mathcal{A}_i^*} \Delta_N^{i+1}$  for  $2 \leq i \leq N$ , with:

$$\Delta_N^i = \begin{vmatrix} -S_{-1}^i & e^{\mathcal{A}_i^*} & 0 & \dots & 0 \\ -S_{-1}^{i+1} & -1 & \ddots & & \vdots \\ \vdots & 0 & \ddots & \ddots & 0 \\ -S_{-1}^N & 0 & \dots & 0 & -1 \end{vmatrix}, \quad \Delta_N^N = -S_{-1}^N, \quad (100)$$

giving  $\Delta_N^2 = (-1)^{N-1} \sum_{i=2}^N S_{-1}^i \prod_{j=2}^{i-1} e^{\mathcal{A}_j^*}$  (note that the latter is in accordance with (92)). We now find that

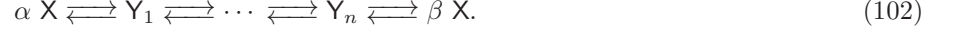
$$e^{n \mathcal{A}^*} \geq \sum_{i=2}^N S_{-1}^i = \mathbf{p}. \quad (101)$$

Throughout all this section we assumed  $\mathbb{S}_+ = \text{Id}$ . If this is not the case, the above results can be generalized by replacing  $\mathbb{S}_-$  by  $(\mathbb{S}_+^{-1} \cdot \mathbb{S}_-)$ , provided  $(\mathbb{S}_+^{-1} \cdot \mathbb{S}_-)$  contains only positive coefficients with a zero diagonal. That will be true if, for example,  $\mathbb{S}^+$  is a diagonal matrix.



### The Generalized Type I

The generalization of Type I networks constitutes a significant class of systems. In this generalization,  $\alpha$  species  $X$  pass through an arbitrary number of linear intermediates of  $Y$  species, giving back  $\beta X$ , ( $\beta > \alpha$ )



For that network:

$$\mathbb{S}_+ = \text{Diag}(\alpha, 1, \dots, 1), \quad \mathbb{S}_- = \begin{pmatrix} 0 & 0 & \cdots & 0 & \beta \\ 1 & \ddots & & & 0 \\ 0 & \ddots & \ddots & & \vdots \\ \vdots & & & \ddots & 0 \\ 0 & \cdots & 0 & 1 & 0 \end{pmatrix}, \quad (103)$$

and the determinant of  $\mathbb{S} = \mathbb{S}_- - \mathbb{S}_+$  is  $(-1)^n(\beta - \alpha)$ . Thus,  $\mathbb{S}$  is invertible if and only if  $\beta \neq \alpha$ , namely, only if (102) is indeed an autocatalytic network. If  $X$  is chemostatted, its elementary mode of production is *i.e.* the first column of  $\mathbb{S}^{-1}$ , which is given by  $\mathbf{g}_X = (\beta - \alpha)^{-1} \mathbf{1} > 0$ , where  $\mathbf{1}$  is a vector of ones. Furthermore,  $(\mathbb{S}_+^{-1} \cdot \mathbb{S}_-)$  has a shape of type (90), and enforcing the determinant of  $\mathbb{M} = \text{Diag}(e^{\mathcal{A}_1^*}, \dots, e^{\mathcal{A}_{n+1}^*}) - (\mathbb{S}_+^{-1} \cdot \mathbb{S}_-)$  to vanish yields

$$e^{(\beta - \alpha)\mathcal{A}^*} = \frac{\beta}{\alpha}. \quad (104)$$

In particular, consider  $\widehat{\mathbf{g}}_X = (\beta - \alpha)\mathbf{g}_X = \mathbf{1}$ , which is the pathway producing  $\beta X$ s starting from  $\alpha X$ s. The overall affinity at  $Q^*$  is always  $\ln(\beta/\alpha)$  or, equivalently,  $Q^* = (\beta/\alpha)K$ . When  $\alpha = 1$  and  $\beta = 2$  one recovers the result derived in the main text for the Type I core.

Going beyond chemical networks, Type I and its generalized version can also be seen as a coarse-grained representation of more general networks and the bounds will be unchanged thanks to a property of network reduction explained in section . below. The overall autocatalytic process can be described by the balance equation  $\alpha X + (\diamond) \longrightarrow \beta X + (\diamond)$ , which we called a seed-dependent mode of production in the main text. We note that if one adds non-zeros terms to lower diagonal of  $\mathbb{S}_-$  in such systems, the property (90) is still verified and the lower bound either stays the same or increases. This shows our conjecture concerning the seed-dependent modes of production for networks without back-branches.

### The Generalized Type II

Looking at Table 1 in Material and Methods of the main text, we notice that the Type II network exhibits a singular behavior when species  $A$  is chemostatted. In that case, the affinity also saturates at  $\ln 2$ , just like for Type I networks. This result is obtained by enforcing  $\det(\mathbb{M}) = 0$ , where

$$\mathbb{M} = \begin{pmatrix} e^{\mathcal{A}_1^*} & 0 & -1 \\ -1 & e^{\mathcal{A}_2^*} & -1 \\ 0 & -1 & e^{\mathcal{A}_3^*} \end{pmatrix}, \quad (105)$$

with  $e^{\mathcal{A}_1^*} = 1$  because  $g_X^I = 0$ . Furthermore,  $g_X^I = 0$  implies that this mode of production is *seed-independent*, as defined in the main text.

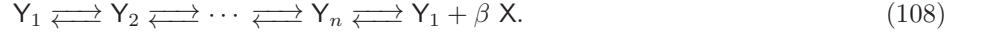
Type II networks represent, in fact, the simplest way of producing  $A$  without the need to have  $A$  initially. This observation motivates the introduction of a generalized Type II network:



which is such that  $\mathbb{S}_+ = \text{Id}$  and

$$\mathbb{S}_- = \begin{pmatrix} 0 & 0 & \dots & 0 & 1 \\ \beta & 0 & \dots & \dots & 0 \\ 1 & 1 & \dots & \dots & \vdots \\ 0 & 0 & \dots & \dots & 0 \\ \vdots & \vdots & \dots & \dots & \vdots \\ 0 & 0 & \dots & 0 & 1 & 0 \end{pmatrix}. \quad (107)$$

In addition,  $\widehat{\mathbf{g}}_{\mathbf{X}} = (1, 0, 1, \dots, 1)^\top$ , which corresponds to the overall stoichiometric equation



This mode represents the simplest network producing  $\beta$  units of  $\mathbf{X}$  with an arbitrary number of  $\mathbf{Y}$  species playing the role of intermediates of reaction.

The matrix  $\mathbb{M}$  reads here

$$\mathbb{M} = \begin{pmatrix} e^{\mathcal{A}_1^*} & 0 & \dots & \dots & 0 & -1 \\ -\beta & e^{\mathcal{A}_2^*} & \dots & \dots & \dots & 0 \\ -1 & -1 & \dots & \dots & \dots & \vdots \\ 0 & 0 & \dots & \dots & \dots & 0 \\ \vdots & \vdots & \dots & \dots & \dots & \vdots \\ 0 & 0 & \dots & 0 & -1 & e^{\mathcal{A}_{n+1}^*} \end{pmatrix}. \quad (109)$$

Expanding along the first row of  $\mathbb{M}$  gives for the determinant  $\det(\mathbb{M}) = e^{\beta \mathcal{A}^*} - (\beta + e^{\mathcal{A}_2^*})$ . The second reaction is not part of the production mode of  $\mathbf{X}$ . It is thus not affected by non-equilibrium constraints and reaches equilibrium. Consequently, we have  $e^{\mathcal{A}_2^*} = 1$ . This yields an analogue of (104) for seed-independent production:

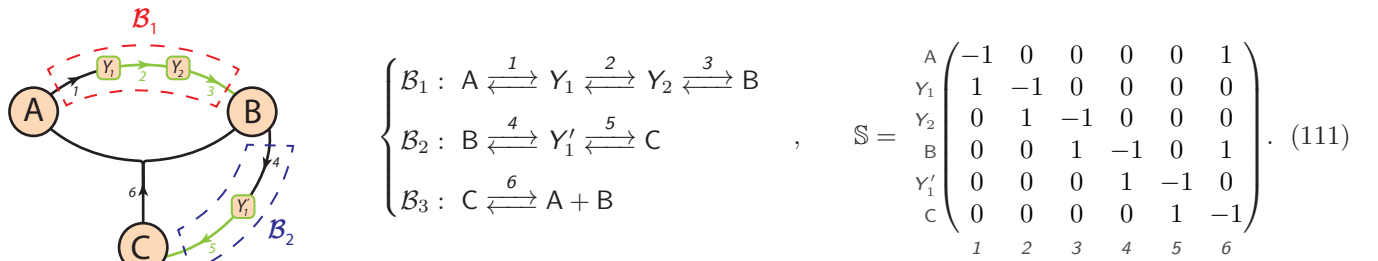
$$e^{\beta \mathcal{A}^*} = \beta + 1. \quad (110)$$

Again, adding terms in the lower diagonal in (107) necessarily increases the bound (110), which supports the conjecture made in the text.

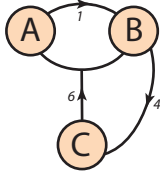
### Network reduction

Here, we show that the overall affinity of a chemical network in the regime of optimal flux considered in this article can be calculated by evaluating it on a smaller network, provided certain conditions are met. By definition, the reduced network contains only *essential species*, and is obtained from the initial network by a coarse-graining procedure, by which non-essential *intermediate species* are removed from the description. For simplicity, let us assume that these intermediate species are present only in linear segments connecting two essential species, which we call *branches*. Before considering the general case, we illustrate below the method using an example with a Type II network.

*Example for the reduction of a Type II-like network* Let us consider the following network, which consists of three branches  $\mathcal{B}_1, \mathcal{B}_2$  and  $\mathcal{B}_3$ :



The only branched reaction is 6 and, in this network, the essential species are  $\{\text{A}, \text{B}, \text{C}\}$ , while the intermediate species are  $\{\text{Y}_1, \text{Y}_2, \text{Y}_1'\}$ . The essential network is:



$$\begin{cases} A \xrightleftharpoons{1} B \\ B \xrightleftharpoons{4} C \\ C \xrightleftharpoons{6} A+B \end{cases}, \quad \mathbb{S}^{\text{ess}} = \begin{matrix} A \\ B \\ C \end{matrix} \begin{pmatrix} -1 & 0 & 1 \\ 1 & -1 & 1 \\ 0 & 1 & -1 \end{pmatrix}, \quad (\mathbb{S}^{\text{ess}})^{-1} = \begin{matrix} 1 \\ 2 \\ 3 \end{matrix} \begin{pmatrix} 0 & 1 & 1 \\ 1 & 1 & 2 \\ 1 & 1 & 1 \end{pmatrix}, \quad \begin{matrix} g_A^{\text{ess}} & g_B^{\text{ess}} & g_C^{\text{ess}} \end{matrix} \quad (112)$$

which is a Type II core. When the chemical network operates in the regime of optimal flux, the following structural relations hold:

$$F_{-1} = F_{+2}, \quad F_{-2} = F_{+3}, \quad F_{-3} = F_{+4}, \quad F_{-4} = F_{+5}, \quad F_{-5} = F_{+6}, \quad F_{-6} = F_{+1} + F_{+4}. \quad (113)$$

From these relations, we can see that the affinity of each branch of the network takes the same value in the original and in the reduced networks, where they are denoted  $\mathcal{A}_i^{\text{ess}}$  for reaction  $i$ :

$$e^{\mathcal{A}(\mathcal{B}_1)} = \frac{F_{-1}F_{-2}F_{-3}}{F_{+1}F_{+2}F_{+3}} = \frac{F_{-3}}{F_{+1}} = \frac{F_{-1}^{\text{ess}}}{F_{+1}^{\text{ess}}} = e^{\mathcal{A}_1^{\text{ess}}}, \quad (114)$$

$$e^{\mathcal{A}(\mathcal{B}_2)} = \frac{F_{-4}F_{-5}}{F_{+4}F_{+5}} = \frac{F_{-5}}{F_{+4}} = \frac{F_{-4}^{\text{ess}}}{F_{+4}^{\text{ess}}} = e^{\mathcal{A}_4^{\text{ess}}}, \quad (115)$$

$$e^{\mathcal{A}(\mathcal{B}_3)} = e^{\mathcal{A}_6^{\text{ess}}}. \quad (116)$$

Let us assume for instance that species A is chemostatted. Its mode of production in the essential network is the following set of reactions :



which means that  $\mathbf{g}_A^{\text{ess}} = (0, 1, 1)^\top$ . Similarly, the corresponding vector for the original network is

$$\mathbf{g}_A = \begin{pmatrix} 0 & 0 & 0 & 1 & 1 & 1 \end{pmatrix}^\top. \quad (118)$$

1   2   3   4   5   6

Note that intermediate species that come between two essential species are described either with a zero entry in that vector if the branch is not present in the mode (for reactions 2 and 3), or with a one if it is present (for reaction 5). Thanks to this property, it is straightforward to relate components of this reaction vector in the original and in the reduced networks.

Then, the initial sum over reactions in the global affinity can be reduced to a sum over affinities of the branches, which as we explained above take the same value in the original and in the reduced networks. It follows from this that the overall affinity in the complete network reduces to its value in the essential network when evaluated in the regime of optimal flux :

$$e^{\mathcal{A}^*} = \exp \left( \sum_{\rho} g_A^{\rho} \mathcal{A}_{\rho} \right) = \exp (\mathcal{A}_4 + \mathcal{A}_5 + \mathcal{A}_6), \quad (119)$$

$$= \exp (\mathcal{A}(\mathcal{B}_2) + \mathcal{A}(\mathcal{B}_3)) \quad (120)$$

$$= e^{\mathcal{A}^{\text{ess}}}. \quad (121)$$

The same property can be shown to hold when other species are chemostatted.

*General case* The general proof follows exactly the same steps as in the example above. We consider a branch  $\mathcal{B}$ , which is defined as the sub-network of  $N$  intermediate species between two essential species  $Z$  and  $Z'$  (see Fig. 4).

The first step is to show that the affinities take the same value for that branch in the original and in the reduced networks, when evaluated in the regime of optimal flux. This follows from the expression of the  $\mathcal{A}_{\rho}^*$ s as a function of the  $F_{\pm\rho}$ s (Eq. (43) of the main text) and the structural relations in a linear segment:

$$\mathcal{A}(\mathcal{B}) = \ln \left( \prod_{i=0}^N \frac{F_{-\rho(i)}}{F_{+\rho(i)}} \right) = \ln \left( \frac{F_{-\rho(N)}}{F_{+\rho(0)}} \right) = \ln \left( \frac{F_{-\rho(0)}^{\text{ess}}}{F_{+\rho(0)}^{\text{ess}}} \right) = \mathcal{A}_{\rho(0)}^{\text{ess}}. \quad (122)$$

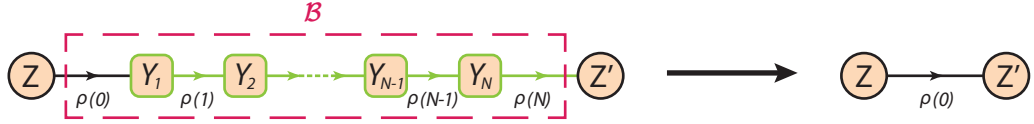


**Figure 4:** The branch  $\mathcal{B}$  between two essential species  $Z$  and  $Z'$  is the sub-network formed by the succession of  $N$  *intermediate species* (represented in green), connected together by unimolecular non-essential reactions (represented in green). The reduction of  $\mathcal{B}$  consists in removing all the intermediates, keeping only the essential species.

From now on we assume that the chemostatted species  $X$  is an essential species that is still present in the network after reduction. The restriction of  $\mathbf{g}_X$  to the reactions in  $\mathcal{B}$  is a constant vector whose values are given by  $g_X^{\rho(0)}$ . Hence, for all reactions  $\rho(i) \in \mathcal{B}$ , the corresponding entry in  $\mathbf{g}_X$  will be  $g_X^{\rho(i)} = g_X^{\rho(0)}$ . Moreover, the entry  $g_X^{\rho(0)}$  is preserved after the reduction:  $g_X^{\rho(0)} = (g_X^{\text{ess}})^{\rho(0)}$ .

As a result, here again, the initial sum over reactions in the global affinity can then be reduced to a sum over affinities of the branches, which take the same value in the original and in the reduced networks. It follows from this that the overall affinity in the complete network equals the value it takes in the reduced network, namely  $\mathcal{A}^{\text{ess}}$ , irrespective of which essential species is chemostatted:

$$e^{\mathcal{A}^*} = \exp \left( \sum_{\rho} g_X^{\rho} \mathcal{A}_{\rho} \right) = \exp \left( \sum_{\mathcal{B}} \sum_{\rho(i) \in \mathcal{B}} g_X^{\rho(i)} \mathcal{A}_{\rho(i)} \right), \quad (123)$$

$$= \exp \left( \sum_{\mathcal{B}} g_X^{\rho(0)} \sum_{\rho(i) \in \mathcal{B}} \mathcal{A}_{\rho(i)} \right) = \exp \left( \sum_{\mathcal{B}} g_X^{\rho(0)} \mathcal{A}(\mathcal{B}) \right), \quad (124)$$

$$= e^{\mathcal{A}^{\text{ess}}}. \quad (125)$$

## FURTHER APPLICATIONS TO SPECIFIC AUTOCATALYTIC NETWORKS

### Bounds for the five simplest autocatalytic motifs

We summarize in Table 1 of the materials and methods of the main text the value of the lower bound on  $\mathcal{A}^*$  for the five simplest autocatalytic motifs described in [20]. Being  $3 \times 3$  (except for Type I that is  $2 \times 2$ ), these networks have a lower bound given by the determinant condition (86) with  $\mathbb{S}_+ = \text{Id}$ . We have checked numerically that (86) is the tightest, except for Type V. In that case, (86) predicts  $(\ln 5)/2$  as lower bound while a numerical simulation shows that the actual one is  $\ln 3$ .

The tightest bound for the Type V motif can be obtained by using the relation provided by the determinant condition and by combining it with the structural constraints (Eq. (25) of the main text). Let us assume without loss of generality due to the symmetry of the network that  $A$  is chemostatted:  $\mathbf{g}_A = (0, 1/2, 1/2)^T$ . As a consequence,  $F_{-1} = F_{+1}$  or, equivalently,  $\mathcal{A}_1^* = 0$  and  $2\mathcal{A}^* = \mathcal{A}_2^* + \mathcal{A}_3^*$ . Now,

$$\mathbb{M} = \begin{pmatrix} 1 & -1 & -1 \\ -1 & e^{\mathcal{A}_2^*} & -1 \\ -1 & -1 & e^{\mathcal{A}_3^*} \end{pmatrix}, \quad (126)$$

and therefore  $\det(\mathbb{M}) = 0 \Leftrightarrow \exp(2\mathcal{A}^*) = 3 + \exp(\mathcal{A}_1^*) + \exp(\mathcal{A}_3^*)$ . From the positivity of  $\mathcal{A}_1^*$  and  $\mathcal{A}_3^*$ , one would predict a lower bound for  $\mathcal{A}^*$  equal to  $(\ln 5)/2$ . On the other hand, the structural constraints read:

$$\begin{cases} F_{-1} = F_{+2} + F_{+3} \\ F_{-2} = F_{+1} + F_{+3} \\ F_{-3} = F_{+1} + F_{+2}, \end{cases} \quad (127)$$

which imply  $e^{\mathcal{A}_2^*} = F_{-2}/F_{+2} = (F_{+1} + F_{+3})/F_{+2}$ , and thus  $x = F_{+3}/F_{+2} = (e^{\mathcal{A}_2^*} - 1)/2 \geq 0$ . Then, the expression for  $\exp(2\mathcal{A}^*)$  can be re-written as:

$$e^{2\mathcal{A}^*} = 3 + \frac{F_{-2}}{F_{+2}} + \frac{F_{-3}}{F_{+3}} = 5 + 2 \left( x + \frac{1}{x} \right).$$

Finally, since  $x + x^{-1} \geq 2$  for all  $x \geq 0$ , we recover that the tightest bound - as confirmed numerically - is :

$$e^{\mathcal{A}^*} \geq 3. \quad (128)$$

We now come back to the specific case of Type I networks. As explained in the main text, chemostatting species B turns the equality,  $\mathcal{A}^* = \ln 2$  into an inequality  $\mathcal{A}^* \geq \ln 2$ . However, Figure 1.C of the main text also shows that the affinity is upper-bounded by  $\ln 4$ , which strongly constrains the location of the extremum of the global rate. This unexpected double constraint can also be obtained using the determinant condition. In that case, the condition on the determinant yields

$$e^{\mathcal{A}_1^* + \mathcal{A}_2^*} = 2. \quad (129)$$

However,  $\mathbf{g}_B = (2, 1)^\top$  also implies that  $\mathcal{A}^* = 2\mathcal{A}_1^* + \mathcal{A}_2^*$ , and  $\mathcal{A}_1^*, \mathcal{A}_2^* > 0$ . Thus, from (129),  $\exp(\mathcal{A}_1^*) = 2 \exp(-\mathcal{A}_2^*) \leq 2$  and similarly for  $\exp(\mathcal{A}_2^*)$ . Hence we obtain:

$$1 \leq e^{\mathcal{A}_1^*} \leq 2, \quad 1 \leq e^{\mathcal{A}_2^*} \leq 2. \quad (130)$$

Multiplying (129) by  $e^{\mathcal{A}_1^*}$  yields the behavior shown in Fig. 1.C of the main text:

$$2 \leq e^{\mathcal{A}^*} \leq 4. \quad (131)$$

### The Hinshelwood autocatalytic cycle

We finish by analyzing the Hinshelwood autocatalytic cycle, which is a model, in which a set of  $n$  enzymes catalyzes each other in a cyclical manner [33]. For  $n = 2$ , this model can be written as :



where  $F_1$  and  $F_2$  are two substrates and  $E_1$  and  $E_2$  are the enzymes. To adapt this model to the framework of [20], we split every reaction above into two consecutive reactions with intermediates  $F_1E_1$  and  $F_2E_2$ . Then, the reactions become



If we now assume that the substrates are in excess and we use the notation  $A = E_1, B = F_1E_1, C = E_2$  and  $D = F_2E_2$ , we obtain the following reaction scheme and stoichiometric matrix :

$$\left\{ \begin{array}{l} A \xrightleftharpoons{1} B \\ B \xrightleftharpoons{2} A + C \\ C \xrightleftharpoons{3} D \\ D \xrightleftharpoons{4} A + C \end{array} \right., \quad \mathbb{S} = \begin{array}{c} A \\ B \\ C \\ D \\ 1 \quad 2 \quad 3 \quad 4 \end{array} \begin{pmatrix} -1 & 1 & 1 & 1 \\ 1 & -1 & 0 & 0 \\ 0 & 1 & -1 & 1 \\ 0 & 0 & 1 & -1 \end{pmatrix}. \quad (134)$$

The matrix inverse is:

$$\mathbb{S}^{-1} = \begin{array}{c} 1 \\ 2 \\ 3 \\ 4 \\ g_A \quad g_B \quad g_C \quad g_D \end{array} \begin{pmatrix} 0 & 1 & 1 & 1 \\ 0 & 0 & 1 & 1 \\ 1 & 1 & 0 & 1 \\ 1 & 1 & 0 & 0 \end{pmatrix}, \quad (135)$$

and the structural constraints are:

$$\begin{cases} F_{-1} = F_{+2} \\ F_{-2} = F_{+1} + F_{+3} \\ F_{-3} = F_{+4} \\ F_{-4} = F_{+1} + F_{+3} \end{cases} \quad (136)$$

Applying the determinant condition on Hinshelwood gives:

$$e^{\mathcal{A}_1^* + \mathcal{A}_2^* + \mathcal{A}_3^* + \mathcal{A}_4^*} - e^{\mathcal{A}_1^* + \mathcal{A}_2^*} - e^{\mathcal{A}_3^* + \mathcal{A}_4^*} = 0, \quad (137)$$

which leads to  $e^{\mathcal{A}^*} \geq 2$ . This bound, while correct, can be improved. If B or D is chemostatted, only the reaction consuming the chemostat (2 or 3) is at equilibrium. As in the case of Type V, the actual value of the bound is obtained using the structural constraints in the relation on  $\exp(\mathcal{A}^*)$  obtained from the determinant condition:

$$e^{\mathcal{A}^*} = \frac{F_{-1}F_{-2}}{F_{+1}F_{+2}} + \frac{F_{-3}F_{-4}}{F_{+3}F_{+4}}. \quad (138)$$

Incorporating the constraints (136) in this expression gives

$$e^{\mathcal{A}^*} = 2 + \frac{F_{+3}}{F_{+1}} + \frac{F_{+1}}{F_{+3}} \geq 4, \quad (139)$$

which is the tightest bound that can be obtained by varying the rate constants as shown on Figure 3.D in the main text.

The situation is drastically different if species A or C are chemostatted. In that case, two reactions are at equilibrium (either 1, 2 or 3, 4), implying that one of the optimal elementary affinities is diverging. Indeed, assuming A is chemostatted, we have  $g_A^1 = g_A^2 = 0$ . This leads to two additional constraints:  $F_{-1} = F_{+1}$  and  $F_{-2} = F_{+2}$ . Thus,

$$\begin{cases} F_{-1} = F_{+1} = F_{-2} = F_{+2} \\ F_{-2} = F_{+1} + F_{+3} \end{cases}, \quad (140)$$

which implies  $F_{+3} = 0$ . On the other hand,  $\exp(\mathcal{A}_3^*) = F_{-3}/F_{+3}$ , obtaining the divergence of  $\exp(\mathcal{A}_3^*)$ . The structural constraints cannot be satisfied and, as a consequence there is no extremum of the global flux within  $]0, +\infty[$ .  $\mathcal{J}(Q)$  is a decreasing function of  $Q$  being maximum at  $Q^* = 0$ . Performing similar reasoning, one shows that controlling C instead leads to a divergence of  $\exp(\mathcal{A}_1^*)$ .

### A bi-stable network: the Schlögl model

We now study the robustness of our approach when bistability is present in the dynamical system. To illustrate this case we analyze the Schlögl model:

$$\begin{cases} A \xrightleftharpoons{1} X \\ 2X \xrightleftharpoons{2} 3X \end{cases}, \quad \mathbb{S}_+ = \begin{matrix} A \\ X \end{matrix} \begin{pmatrix} 1 & 0 \\ 0 & 2 \end{pmatrix}, \quad \mathbb{S}_- = \begin{matrix} A \\ X \end{matrix} \begin{pmatrix} 0 & 0 \\ 1 & 3 \end{pmatrix}, \quad \mathbb{S}^{-1} = \begin{matrix} 1 & 2 \\ 2 & 1 \end{matrix} \begin{pmatrix} -1 & 0 \\ 1 & 1 \end{pmatrix}. \quad (141)$$

$g_A \quad g_X$

Usually a second reactant B is found in the second reaction  $2X + B \xrightleftharpoons{2} 3X$ . The latter is an *external species*, whose concentration is absorbed in the effective rate  $k_{+2}$  and we do not note it explicitly for this reason.

It is well-known that controlling the concentration of A in such network can result in bistable solutions for the stationary concentration of X,  $x$ . Indeed the latter obeys the following cubic equation:

$$-k_{-2} x^3 + k_{+2} x^2 - k_{-1} x + k_{+1} Q = 0, \quad (142)$$

where  $Q$  is the concentration of A that is also the reaction quotient. The cubic discriminant of (142) is:

$$\Delta = -27 k_{+1}^2 k_{-2}^2 Q^2 + 2 k_{+1} k_{+2} (9 k_{-1} k_{-2} - 2 k_{+2}) Q + k_{+2}^2 k_{-1}^2 - 4 k_{-1}^3 k_{-2}. \quad (143)$$

If  $\Delta \geq 0$ , (142) has 3 real solutions, and if  $\Delta < 0$  (142) has only 1 real solution. The third order discriminant (143) is a second order polynomial in  $Q$ . Its sign depends on the sign of the second order discriminant  $\delta = 16 k_{+1}^2 (k_{+2}^2 - 3 k_{-1} k_{-2})^3$ . If  $\delta > 0$  (resp.  $\delta < 0$ ) then (143) will be positive (resp. negative) if  $Q$  lies between (resp. outside) the two real roots of (143). In the bistable region where  $\Delta > 0$ , (142) two of the solutions to the third-order polynomial correspond to stable states, and the third one is an unstable state. Consequently, there will be two different stable fluxes in this parametric region (see Figure 5).



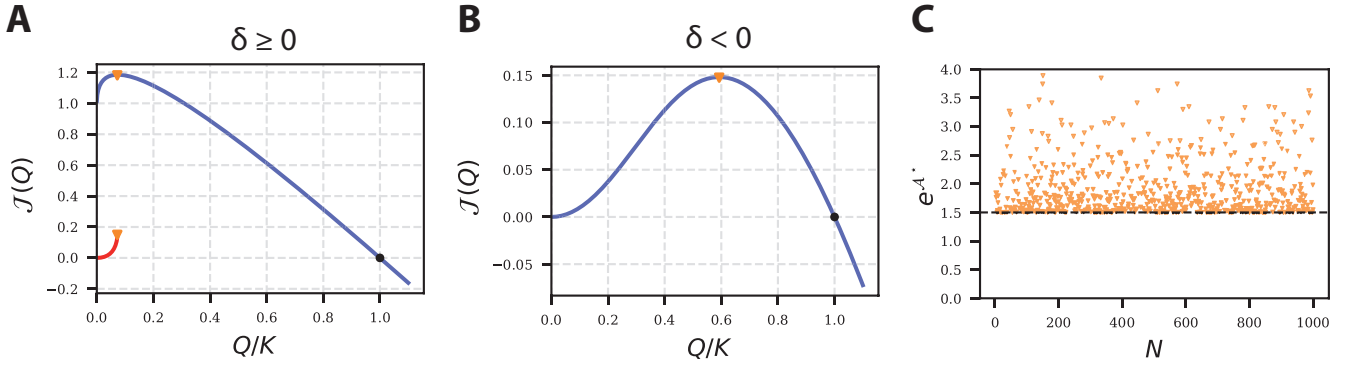


**Figure 5:** The location of the extremal flux of the Schlögl cycle also exhibits a lower bound. **A** When the second-order discriminant  $\delta$  is positive, the third order discriminant (143) will have a positive region in which two values of the macroscopic flux co-exist (these curves were obtained for  $k_{-1} = k_{-2} = 1$ ,  $k_{+1} = 0.1$ ,  $k_{+2} = 2$ ). **B** If  $\delta$  is negative, (142) has only one real root yielding a unique solution for the macroscopic flux (the curve was obtained for  $k_{+1} = k_{+2} = k_{-2} = 1$ ,  $k_{-1} = 2$ ). In both cases the macroscopic fluxes vanish at equilibrium (solid black circle) and have a maximum (solid black square). **C** The affinity at the maximum of the flux for randomly chosen kinetic constants (solid orange marker) are lower-bounded by  $3/2$  (dotted black curve), as predicted by (145).

The matrix  $\mathbb{M}$  is here given by

$$\mathbb{M} = \begin{pmatrix} e^{\mathcal{A}_1^*} & 0 \\ 0 & e^{\mathcal{A}_2^*} \end{pmatrix} - (\mathbb{S}_+^{-1} \cdot \mathbb{S}_-) = \begin{pmatrix} e^{\mathcal{A}_1^*} & 0 \\ -1/2 & e^{\mathcal{A}_2^*} - 3/2 \end{pmatrix}. \quad (144)$$

The condition  $\det(\mathbb{M}) = 0$  yields  $\exp(\mathcal{A}_1^* + \mathcal{A}_2^*) = (3/2)\exp(\mathcal{A}_1^*)$ . In addition, because  $\mathbf{g}_A = (-1, 1)^\top$ , the cycle affinity at steady-state is  $\mathcal{A}^* = \mathcal{A}_2^* - \mathcal{A}_1^*$ . This leads to the following lower bound:

$$e^{\mathcal{A}^*} = \frac{3}{2}e^{-\mathcal{A}_1^*} \geq \frac{3}{2}. \quad (145)$$

Our formalism applies to situations where the derivative of the flux is zero. This can happen only for the branch associated to the solution of (142) which has the highest rate. The lower flux is an ever-increasing function of  $Q$  (see Fig. 5A). As a consequence, it will reach a maximum at the transition between the bistable region and the monostable region, where the corresponding steady-state disappears.